2015-06-01

Void Modeling in Resin Infusion

Mark Wesley Brandley
Brigham Young University - Provo

Void Modeling in Resin Infusion

Mark Wesley Brandley

A thesis submitted to the faculty of
Brigham Young University
in partial fulfillment of the requirements for the degree of

Master of Science

Andrew R. George, Chair
Michael P. Miles
David T. Fullwood

School of Technology

Brigham Young University

June 2015

ABSTRACT

Void Modeling in Resin Infusion

Mark Wesley Brandley
School of Technology, BYU
Master of Science

Resin infusion of composite parts has continually been reaching to achieve laminate quality equal to, or exceeding, the quality produced with prepreg in an autoclave. In order for this to occur, developers must understand the key process variables that go in to producing a laminate with minimal void content.

The purpose of this research is to continue efforts in understanding 1) the effect of process conditions on the resultant void content, with a focus on resin infusion flow rate, 2) applying statistical metrics to the formation, location and size of voids formed, and 3) correlation of these metrics with the local mechanical properties of the composite laminate.

The variation in dispersion and formation of micro-voids and macro-voids varied greatly between the rates of flow in which the infusion occurred, especially in the non-crimp carbon fiber samples. Higher flow rates led to lower volumes of micro-voids in the beginning section of the carbon fiber laminates with macro-voids being introduced approximately half-way through infusion. This was determined to have occurred with the decreasing pressure gradient as the flow front moved away from the inlet. This variation in void content per location on the laminate was more evident in the carbon fiber samples than the fiberglass samples.

Micro-voids follow void formation modeling especially when coupled with a pressure threshold model. Macro-void formation was also demonstrated to correlate strongly to void formation models when united with void mobility theories and pressure thresholds.

A quick decrease in mechanical properties is apparent after the first 1-2% of voids, signaling strength is mostly sensitive to the first 0-2% void content. A slight decrease in SBS was noticed in fiberglass laminates, A-F, as v_0 increased but not as drastically as represented in the NCF laminates, G and H. The lower clarity in the exponential trend could be due to the lack of samples with v_0 greater than 0% but less than 1%. Strength is not well correlated to void content above 2% and could possibly be related to void morpholology.

Keywords: Mark Brandley, resin transfer molding, void formation, process optimization, out-of-autoclave, carbon fiber, vacuum infusion, resin infusion

ACKNOWLEDGEMENTS

I would like to thank Dr. Andrew George for all of his time, patience and efforts as he imparted his knowledge with me to develop this thesis and my love for composite materials processing. His excitement for the topic was contagious and encouraged me to continually strive to learn and do more.

The entire School of Technology faculty and Dr. Fullwood played a significant role in helping me complete this thesis and I appreciate each and every one of their efforts keeping me focused and lending a hand whenever needed.

My gratitude for Plasan Carbon Composites for supporting me through the final steps of my research and for sharing with me their expertise and wisdom gained in the field of composites processing development.

Lastly, my heart is full of gratitude for the support, patience and understanding of my family. Laci has supported me from the beginning and has been a key contributor to my success in this program. I am grateful for the sacrifices that my wife and child have made on my behalf along with my mother, father and sibling's encouragement as I fulfill my dreams. I truly appreciate everyone's support and efforts in understanding the importance of this research to me.

TABLE OF CONTENTS

LIST OF TABLES

LIST OF FIGURES

1 INTRODUCTION

As composite materials become more and more prevalent in today's world, the ability to process them cheaper and faster while maintaining their key strength characteristics becomes increasingly important. The strength of a laminate not only depends on the design but how well each layer is consolidated together. Processes for constructing composite laminates focus on consolidation and the removal of volatiles and air that could be trapped in between the fibers. Voids, or air bubbles trapped in the cured laminate, greatly influence the overall mechanical characteristics of the laminate.

Currently the major process that consistently produces composite laminates with a homogenous void content of less than 2% is through high-pressure autoclave-prepreg processing. Although high pressures in an autoclave provide the energy to compact layers and remove voids, it comes at a steep cost. Autoclaves are notorious for lengthy processing times, expensive equipment and pre-impregnated material. All of these variables increase the cost of the product. The need to produce the same quality of laminate as an autoclave at a reduced cost is driving a large amount of research and development into out-of-autoclave (OoA) technologies. Much of this research has focused on resin infusion processes, particularly resin transfer molding (RTM).

Resin infusion (RI) processing covers a number of different processes that start with a dry fibrous reinforcement that is then infused with resin. In RTM, dry fibers are placed in an enclosed, matched mold and resin is infused into the fibers through a high-pressure system.

Other forms of resin infusion processing, such as vacuum infusion (VI), use vacuum pressure to pull the resin into the fibers rather than use over-pressure to inject the resin. The use of dry fibers reduces material costs, allows greater flexibility in preforming and material choice, and eliminates the need for costly freezers required by pre-impregnated fibers, i.e. prepreg.

Resin infusion processes are most often done without the assistance of an autoclave oven, thus resulting in a more cost effective and faster process than the autoclave-cure required by many prepreg materials. Decreased cost is attributed to the reduction in manual, hand layup processing through the use of "preforms", which reduces cycle time. A preform is multiple layers of dry fabric that are held together with a heat-activated binder. Multiple layers are placed in a preform die that is then heated, creating a preformed shape of the part. Thick parts can be built up quickly by simply adding more dry fiber during the preform process.

The goals of resin infusion processing research are to produce laminates of the same quality as autoclave processing – minimal voids and high fiber to resin ratios. Voids are formed during the process of resin infusion when the resin is infused into the fibers. As the resin flows in-between the fibers, air bubbles are occasionally trapped and frozen in place once the resin cures. These bubbles (voids) form areas that will increase the chances of crack initiation as well as crack propagation, which contribute to failure of the part. In composite laminates and void modeling there are two types of voids that are referred to: macro-voids and micro-voids. Macro-voids are defined as voids that form in between the tows, or rovings, in a laminate while micro-voids are those that form between the individual filaments that the tow is comprised of. The creation and final disposition of voids is difficult to determine but is essential in the creation of models that will accurately predict and characterize voids in RTM laminates.

1.1 Problem Statement

The lack of understanding to predict the cured-in-place void distribution and the void content's effects on the mechanical properties in a resin infused laminate is a major drawback in the realization of industry adopting resin infusion processing. The effects of voids on composite laminates constructed with autoclave-prepreg processes have already been extensively studied. These studies have enabled many models to be established that predict the mechanical properties of the laminate. The prediction of mechanical properties in autoclave-prepreg laminates is simplified given the typical homogeneous void distribution. A homogeneous void content in autoclaved laminates is typical due to the consistent pressure across the entire surface of the part during cure. Numerous papers and studies have shown that certain void percentage (v_0(%)) gives certain shear or tensile properties, but few exist for the heterogeneous void distribution typical in RTM laminates.

The void distribution in resin infused laminates varies with resin movement from one end of the part to the other and the resultant pressure gradient along the flow path. The pressure gradient in resin infusion does not promote homogenous void formation like typical autoclave processes. Voids form at different rates as resin flows at varying velocities. The velocity of the resin depends on the pressure it is infused at along with the interaction of the resin with the fiber at the flow front, a phenomenon described by porous media fluid dynamics theory. To predict a part's final mechanical properties, the final cured part's void content must be known, including: concentration, size and distribution. Despite the progress in void formation modeling, no one can relate these variables to the final mechanical properties until bubble formation is coupled with bubble movement and dispersion before resin cure.

1.2 Research Questions

The purpose of this research is to understand the effect of processing conditions on the concentration, location and distribution of voids in a resin transfer molding composite laminate as well as the influence of those voids on the resulting mechanical properties.

1.3 Hypothesis

It is hypothesized that adjusting infusion pressure in RTM, which in turn alters the infusion velocity, to some optimum value, will result in a laminate with little to no void content comparable to autoclave-prepreg laminates. Many researchers have attempted void formation modeling but no one can relate these models to the final mechanical properties in the laminate.

Therefore, it is hypothesized that process conditions, like the flow-rate, can be related to prediction of void formation. As a result, process variables can be used to allow prediction of Short Beam Shear of composites made through RTM.

1.4 Methodology

1.4.1 Materials

Various fabric reinforcements were studied in this work. The fiberglass fabric studied is an unbalanced weave, JB Martin TG-15-N (with PPG roving). Two types of carbon fiber fabrics were utilized in the testing: 1) a generic aerospace-grade uni-directional (UD) weave with thin glass rovings woven in the weft direction and 2) a biaxial non-crimped fabric, VectorPly C-BX 1800. The JB Martin fabric laminates were cured with Rhino Epoxy 1411 with 4111 Hardener. The carbon UD weave was cured with Hexcel RTM-6 epoxy resin. The tooling for the fiberglass laminates was manufactured from aluminum 6061. The pressurization system was a homemade

system made from a standard pressure pot and connected to house-supplied pressurized air. Two Memmert ovens were used for curing and moisture removal. Density testing prior to combustion testing was performed with a Mettler Toledo micro analysis scale along with a density kit for weighing submersed samples. Combustion samples were processed in a high-temperature gas furnace. Microscopy samples were polished with standard metallographic methods of successive grinding and polishing at decreasing grit sizes. Micrographs were imaged and analyzed using a Zeiss AxioObserver A1M microscope and a Sony SLTA77V-a77 Digital SLR camera.

1.4.2 Experimentation

Fiberglass laminates were prepared by RTM at 3 different infusion pressures: 0.75, 1.00, 1.20 Bar. The resin was infused into five layers of 400 x 300 mm fiberglass fabric. The pressure was monitored to maintain a constant pressure of the set value throughout the infusion. Once the resin reached the outlet, the inlet and vent tubes were immediately closed before oven treatment for cure.

Permeability of the fiberglass and carbon fiber fabrics was studied for the purpose of determining the coefficient of permeability, K, for equations, including Darcy's Law (Darcy 1856), to solve resin flow through the specified fabric. This was performed via vacuum infusion of a Newtonian fluid (canola oil) and timed to determine rate of flow at a given vacuum pressure through a specified thickness and orientation of fiber.

Non-destructive testing was performed via C-Scan Attenuation to provide a comparison set of data for void location. This data was compared to data gathered through microscopy analysis, combustion testing, as well as attempts of macro-lens photography methods developed in-house. This data will also provide data to assist in modeling the creation and movement of voids along the resin flow front during infusion.

Mechanical properties of the cured laminate were tested through ASTM D 2344/D 2344M-00, Standard Test Method for Short-Beam Strength (SBS) of Polymer Matrix Composite Materials and Their Laminates. SBS tests were carried through on an Instron 5569A test structure with Bluehill operating software.

Infusions by RTM of the carbon UD weave were performed prior to this study by other laboratories, as well as c-scan measurement and interlaminar shear strength (ILSS) testing, but the resulting data was analyzed as part of this study. All laminates analyzed in this study are listed in Table 1-1.

Table 1-1: Laminate Labeling Method

Laminate	Infusion Pressure/Flow Rate	Material
A	0.75 bar	Fiberglass
B	0.75 bar	Fiberglass
C	1.00 bar	Fiberglass
D	1.00 bar	Fiberglass
E	1.20 bar	Fiberglass
F	1.20 bar	Fiberglass
G	100 cc/min	Carbon UD weave
H	400 cc/min	Carbon UD weave

1.5 Delimitations and Assumptions

The pressures chosen were not decided upon by calculation and determining optimal velocity for resin infusion. Rather, three infusion pressures were chosen given the capabilities of

the infusion equipment that represent a low, middle and high infusion range. Using the range of infusion pressures, conclusions may be drawn on the effects of resin infusion and its effect on void creation and movement. It is expected that void formation, quantities and movement will vary for each infusion pressure. Two types of material were tested and void models formed from the characteristics of each material. Each material will exhibit its own behavior under infusion environments.

1.6 Definitions and Terms

Flow processing – general term that refers to any composite laminating process that utilizes either vacuum- or over-pressure to infuse resin into dry fibers

Macro-void – bubble or air gap formed in between tows, or rovings during infusion

Micro-void – bubble or air gap formed between filaments inside a tow, generally smaller than a macro-void

Out-of-Autoclave – (OoA) refers to production of composite laminates without an autoclave that are capable of achieving similar properties to those that are produced in an autoclave

Preform – an assemblage of reinforcement plies shaped to be near the final shape of the product while only lacking resin cure

Race tracking – a situation when resin takes the path of least resistance and travels at a higher velocity then the resin flowing through the fiber bundles and typically reaches the resin outlet, which causes a disruption in the flow of the remainder of the infusion

Resin Transfer Molding – (RTM) is a composite molding pressure where over-pressure and typically vacuum work together to push and pull resin through a dry fiber preform

SBS – Short-Beam Strength

v_F – refers to fiber volume content which is typically given as the volume of fiber divided by the total volume (including resin and voids)

v_{0M} – macro-void volume content

v_{0m} – micro-void volume content

v_0 – Void volume content – similar to fiber content, this is measured as the volume of voids in a samples divided by the total volume of the sample.

Void – air bubbles that are trapped in a laminate after cure

2 LITERATURE REVIEW

2.1 Introduction

Recent research in the flow processing community has proposed a relationship between the flow-rate in resin infusion processes and void creation. This is a fluid mechanics approach to describing bubble formation by mechanical entrapment. These studies will not become useful to the simulation of resin infusion processes until this data of void formation can be paired with models for void mobility and predictions of final void distribution in an infused laminate. Additionally, void formation, mobility and final distribution needs to be studied along with the effects of such voids on a composites' mechanical performance.

This literature review will provide background on previous research performed regarding void formation, mobility and final distribution along with the "effects of defects" in composite laminates. The desire is that this research will contribute to providing a more detailed description of voids and describe their effects on the mechanical properties in resin infusion.

2.2 Void Measurement Methods

The simplest method in execution to measure v_0 is related to Test Method II in ASTM D3171. An approximate volume of all solids and voids is calculated by multiplying the measured thickness by the laminate's length and width. The weight of fiber comes from measurement of the weight of the dry preform before infusion. The weight of the resin is the

difference between the weight of the cured laminate and the dry preform. The actual volume of all solid components, fiber and resin, is then calculated from the densities of each component. The difference between these two volumes, with voids and without voids, is the volume of air.

This method gives an easily obtained bulk measurement of v_0 without the need for many tests of the same sample. It relies on many approximations: the individual densities of the components can be difficult to accurately measure, and the rounded edges and irregular thickness of the cured laminate depart from the assumed ideal geometry.

A more contained version of this method requires determining the density of a small sample as well as its mass of resin and fiber. The density is usually determined by either a pycnometer or weighing while immersed per ASTM D792. The sample volume is then determined from the sample mass and the density. ASTM D3171, Method I, is then followed by measurement of the constituent content masses through either digestion or combustion. Digestion methods involve dissolving the resin from a laminate sample. The sample's weight before digestion and the weight of the remaining fibers are compared with the samples pre-digestion density. This method entails little subjectivity, but the void size and location cannot be characterized and it requires the use of hazardous chemicals. Combustion works similarly to digestion and does not require the chemicals but has proven to cause errors with carbon fibers as carbon may char at the temperatures typically used to burn off the resin.

Optical microscopy of voids has been the most popular of v_0 measurement methods (Liu 2006, Cann 2008). A sample is cut from the laminate, polished and then examined under a microscope. Voids should appear as the darkest areas in a sample image from light microscopy. This enables an operator to perform a percentage calculation of dark versus light space to determine the void content. A gray-scale threshold must properly delineate the void areas. A

clear threshold definition of voids requires fine polishing of each sample. The polishing equipment available in many labs often limits the ability to use this method. Both intra-tow micro-voids and inter-tow macro-voids are difficult to delineate with an automated threshold algorithm as they represent a small percentage of the gray scale and are only slightly darker than the resin. Intra-tow micro-voids are particularly difficult to characterize, as they are small enough to resemble usual polishing artifacts and can be difficult to delineate from resin pockets.

Ultrasonic c-scan inspection is a non-destructive technique (NDT) to detect defects and has been used for v_0 measurement (Liu 2006). Optical microscopy results for void measurement can be reasonably correlated with data collected in ultrasound c-scan measurement processes. Ultrasound's non-destructive test method has gained appeal to determine void content in composite laminates. The local attenuation gathered from a c-scan measurement can be compared to a microscopy sample originating from the same location in the sample. The local attenuation increases in a roughly linear trend with increasing macro-void concentration, as the air porosity dampens the signal. This correlation serves as the basis of general ultrasound non-destructive testing of composites.

2.3 Void Formation Modeling

The reinforcement of most high-performance composite parts consists of several fiber bundles (i.e. tows, roving or yarns) held together in individual fabric plies. The resin flow in such a fabric can be described as dual-scale: having both a macro-scale and micro-scale. Similar to the two classifications of voids, the macro-scale flow is inter-bundle, while micro-scale flow is intra-bundle. Intra-bundle refers to interactions between the individual fibers themselves inside the bundle. The velocity of macro-flow is largely determined by the applied pressure gradient, while micro-flow velocity is largely determined by capillary forces due to the

thousands of tightly packed fibers in each bundle (Ahlborn 2009). This often causes a non-uniform flow front, termed "fingering," referring to the different filling velocities in the bundles and between them (Figure 2-1).

Figure 2-1: Dual-Scale Flow "Fingering": Along Stitching Fibers (Left) and in Between Tows (Right).

In flow experiments, the flow-capacitance of the reinforcement, or permeability, has often shown to vary with filling velocity, which complicates flow simulation efforts (Kim 2007). If other conditions are the same, this difference in measured permeability is generally believed to be attributable to capillary forces arising from such dual-scale reinforcements usually used in resin infusion (Ahn 1991, Lai 1997). This capillary-induced difference in flow rates at the macro-scales and micro-scales has also been linked to the void formation by mechanical entrapment. Mechanical entrapment refers to the void formation process that occurs as the dry fiber preform is wetted through resin flow. With the increased importance of low porosity OoA manufacturing processes, and higher accuracy in filling simulation, these dual-scale effects have become the subject of many recent investigations.

Patel and others theorized and proved to a degree that low macro-flow velocities produce macro-bubbles between the fiber bundles. This occurs when micro-, i.e. capillary-flow outruns the macro-flow. In the opposite case, high macro-flow velocities produce micro-voids within the

bundles (Patel 1996, Leclerc 2008). There then exists an optimum filling velocity for a particular fabric-matrix combination, which results in the minimum of both macro-voids and micro-voids (Figure 2-2). The optimal velocity is when the applied pressure gradient causes the macro-flows and micro-flows to travel at roughly the same speed, resulting in a uniform flow front across the two scales (LeBel 2014).

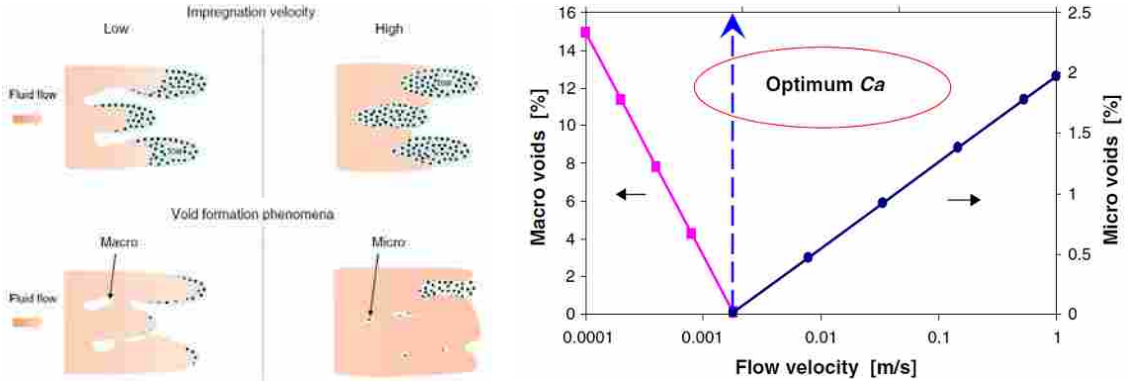

Figure 2-2: Void Formation by Location as Resulted to Filling Velocity (Left) and Optimum Velocity for Minimum Voids (Right), Reprinted from (LeBel 2014)

Determining the flow of resin through a fiber preform is required for modeling void formation and typically determined through application of Darcy's Law (equation 2-1):

$$v = \frac{K}{\mu\phi}\nabla P \tag{2-1}$$

Darcy's law implies that the velocity of the resin flow is related to the permeability of the material, K, the viscosity of the resin, μ, the porosity of the material, ϕ, and the pressure gradient ∇P.

Many models to simulate such void formation have recently appeared including implementation of this to filling simulation for void minimization (Ruiz 2006, Garcia 2010,

Lawrence 2009). The experimental work to validate these void formation models have focused on either *a priori* or *in situ* evaluations of void generation. The *a priori* methods employ textile and fluid dynamics modeling to calculate analytical predictions of the optimum velocity (Gourichon 2006, Park 2011, Lee 2006, LeBel 2014). *In situ* methods investigate void generation at the flow front during infusion. This has been accomplished by: measuring pressure changes at different flow rates, comparison of flow-rates at the inlet and at the flow front or by light transmission, electrical conduction or thermal conduction (Verrey 2006, Gourichon 2006, LeBel 2012, Michaud 2007, Ravey 2013, Villiere 2013). Light transmission seems to be the most robust of these experimental methods for fiberglass but is impossible with opaque carbon fibers. It becomes increasingly difficult to measure void formation rates at varying pressures as well due to the availability of transparent tooling that is capable of being monitored while an infusion is taking place. Current trends point to higher pressure resin infusions that cannot be simulated without closed-molded tooling. Some of the aforementioned methods show only void formation in the outer ply and not through-thickness or between filaments. Large amounts of voids will be formed between the layers as compaction levels of fibers increases, also increasing chances of entrapment of bubbles.

2.4 Void Mobility Modeling

Despite the progress in void formation modeling, no one will be able to relate these models to the final mechanical properties until void formation is coupled with void movement and dispersion before resin gelation. Separate phenomena in void movement and dispersion have been addressed in fluid dynamics studies. For macro-voids formed by slow inter-bundle flow, the pressure gradient in the channel makes the smaller voids continue to move towards the flow front. Larger voids become trapped in the inter-bundle gaps until the rising pressure causes them

to split or shrink – per the Ideal Gas Law – to a critical size where they can escape and flow quickly to the flow front where they dissipate and disappear (Patel 1996, Gourichon 2006, Park 2011).

Micro-bubbles formed by fast inter-bundle flow more likely remain stuck in the dense fiber bundle until the rising pressure makes them shrink or dissolve (Henry's Law for diffusion) to a critical size for mobilization, at which point they escape to the inter-two channels and also move quickly to the flow front (Lundstrom 1997). All voids moving within the inter-bundle gaps are impeded by fiber adhesion forces and mechanical obstructions like stitching threads (Lundstrom 2010). As the pressure increases throughout the infusion, the voids continue to shrink and dissolve into the resin, and there remains a small contribution to this diffusion by convection for the moving bubbles (Lundstrom 1997).

Few experimental studies exist with attempts at coupling these effects together and then coupling them to void formation models to predict the final void content (Lundstrom 2010, Frishfelds 2007). These attempts are hindered by the complexity of the approaches and the multi-disciplinary nature of the coupled models. Therefore, work remains to allow viable use of void prediction in filling simulation.

2.5 Mechanical Effects of Voids

In order to predict a part's final mechanical properties, the final cured part's void content must be known (i.e. void distribution, concentration, and size). Many experimental studies exist that relate mechanical properties to void content in composite laminates but these papers largely focus on voids formed through autoclave processed composite laminates. Homogenous pressure across the laminates surface creates an environment conducive to a consistent void content in any

given section. Resin infused laminates vary in that the pressure gradient across the laminate varies given the flow front's position in the laminate and its distance from the infusion point.

Recent attempts to relate void content to mechanical properties for LCM laminates have been performed but lack depth and do not provide enough data relating the modeling of voids and void types to mechanical failure such as shear strength. In one such study, tensile data collected varied nicely with void content as suspected but only a single tensile sample was taken for each measurement point (LeBel 2014). Lack of repeatability for statistical analysis leaves little confidence in the results. Other studies clearly look at standard tensile tests and fail to measure bending strength of a laminate This paper presents an approach to understanding the final disposition of voids in a heterogeneous environment and their individual effects on the laminate's mechanical properties as well as whether this can be predicted given a laminate's fabric/matrix composition.

3 EXPERIMENTAL DESIGN

3.1 Permeability Measurement

3.1.1 1D Permeability Measurements

1D permeability is determined through a uni-directional flow infusion test. Fabric specimens in these experiments were cut to 200 x 100 mm and stacked 4 plies thick. Permeability tests were run at different fiber orientations: 0^o, 90^o, and 45^o with all plies in each test in the same orientation. Once laminates were prepared, they were placed on a steel caul plate where a precise process was followed to promote proper permeability measurements (see figure 3-1).

Figure 3-1: 1D Permeability Test Fixture

Vacuum bagging “tacky-tape” was placed around the borders of the caul plate touching the edges of the fiber laminate so no air paths were present, preventing race tracking from occurring. After tacky-tape was in place, flow media was placed touching each end of the underside of the sample. The inlet side had an additional layer of flow media to bring resin to the topside of the laminate as well. A spiral cut inlet hose was placed on the flow media covering the width of the laminate and a standard hose was fed into the center of the spiral hose. A simple hose was placed on the opposite side of the laminate to provide vacuum.

A vacuum bag was then placed over top of the laminate making sure to prevent any creases which would also provide paths for race tracking to occur. Vacuum was pulled and measured to confirm that few enough leaks were present that a minimum of 5 mBar pressure was maintained inside the mold. Vacuum was turned off and timed to be sure no significant drop in vacuum over one minute time. Ambient pressure and pressure of vacuum were recorded as well as temperature. The next step was to limit the fluctuation in the vacuum bag height (mold thickness) that occurs as the resin flows into the laminate and lifts the bag. This fluctuation was controlled by snuggly clamping a large block of acrylic to the topside of the laminate and shimmed to provide equal thickness of the laminate. Three laminate thicknesses were tested: 2.04, 2.14 and 2.24 mm. A metric ruler was placed on the top of the acrylic to allow measurement of flow.

The inlet side was then connected to a cup of Canola Oil while constant vacuum was being pulled. A timer was started as soon as the “resin” reached the laminate. Time was recorded at each increment of 10 mm that the resin wet out the laminate. Caution must be taken with measurements as any variation in the angle the ruler is viewed could skew data. This was continued until the entire fabric sample was wet-out or until 30 minutes was reached, whichever

occurred first. This allows for determination of the K_x and K_y variables but not K_z. K_x represents the permeability of the fabric along the length or direction of infusion, while K_y references the permeability of the fabric perpendicular to the direction of the infusion. K_z relates to the through-thickness permeability of the material.

3.1.2 3D Permeability Measurements

A new method for K_z measurement was developed and presented along with the K_z results used in this thesis (George 2014). A two-part tool was constructed out of 300 x 300 x 100 mm acrylic blocks (see figure 3-2). The blocks were machined with an inlet hole with a fitting in the center in the tool with a vent hole located 70 mm from the center point. A silicone seal was attached around the perimeter of the 150 x 150 mm cavity to create an enclosed cavity. Holes for eight grade-8 bolts were drilled into the perimeter of the tool to compress seals and retain pressure in the vessel. The distance of separation and control of compression of material between tool halves A and B was determined by shims of predetermined thickness: 2.04 mm, 2.14 mm and 2.24 mm.

The outlet hole was sealed off for pressurization prior to infusion to test the sealing of the mold. For the test infusion, the vent was left open to the atmosphere, while the inlet was attached to the pressurized resin pot. Pressure was applied through a standard painting pressure vessel with a pressure gauge and valve to control applied pressures. A hose was placed in the pressure vessel and reached to a cup of canola oil. Tests were performed on both the fiberglass and carbon biaxial NCF fabrics with set ply counts and overall thicknesses.

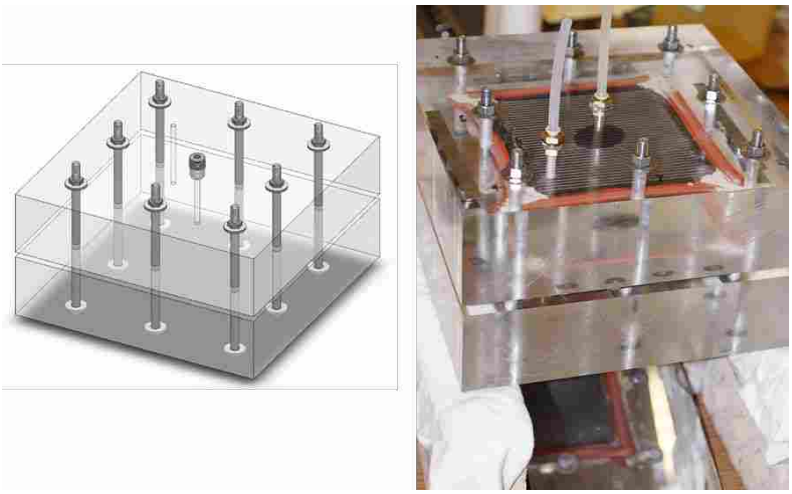

Figure 3-2: 3D Permeability Test Fixture Displaying 3D Model (Left) and Flow Front During Infusion Experiment (Right).

The process was performed by placing the predetermined fiber into the cavity being cautious to not break the seal with any fibers that could lead to a leak of material. Tool temperature was then measured. The pressure vessel was set to 1 bar overpressure and checked via its gauge for leaks in tooling. When no leaks were present, the oil was released and allowed to flow into the tool. The timer was started once oil reached the fabric.

The optically clear mold material allows for observation of the resin permeating the fibers on the surface of the reinforcement stack, as well as when the resin touches the bottom surface after infusing through the entire thickness of the sample and reaches the underside of the tool. Once the oil reached the underside of the fabric the timer was stopped, the ellipse on the top surface (Figure 3-2) was marked and measured, and pressure was released.

3.2 Resin Transfer Molding and Laminate Preparation

3.2.1 Tooling

A mold cavity measuring 400 x 300 x 2 mm was machined into tool-side B out of 6061 aluminum (Figure 3-3). A 300 x 5 x 4 mm resin channel along both the inlet and outlet sides ensures an even resin flow front during infusion. Tool-side A contained an inlet and outlet machined at the center-point of the resin channel. Each hole was tapped to allow quick-connect fittings to secure 8 mm diameter tubing. A 4 mm channel around the outer edge of the tool contained a 5 mm silicone belt to seal the cavity. The two mold halves were secured with 16 grade-8, 9/16 inch bolts tightened in a sequenced pattern to guarantee consistent clamping pressure. The tool was sealed and released with Chem-Trend Chemlease release agent.

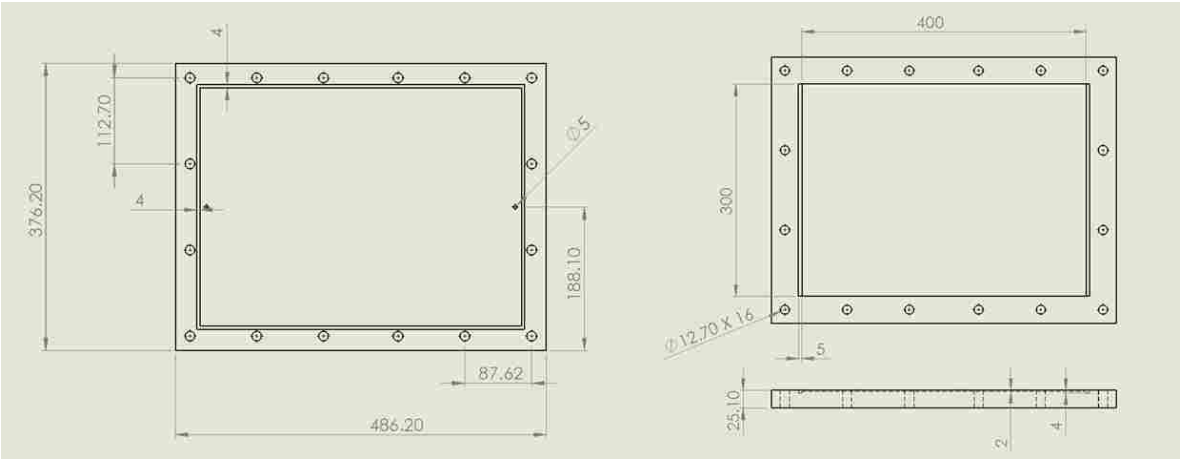

Figure 3-3: RTM Tooling Tool-side A (Left) and Tool-side B (Right)

3.2.2 Pressurization System

A pressurization system was manufactured using a standard 2.5-gallon air pressure paint tank. The paint tank was converted with a controllable pressure valve and inlets to accept the standard 12 mm diameter hoses.

3.2.3 Fiber Orientation and Sample Layup

Laminates were made by RTM with Hexcel RTM-6 and the generic carbon UD-weave by Applied Composites AB ACAB in Lynkoping, Sweden. The data retrieved from these panels was employed in this study. To compare void modeling between carbon and fiberglass, laminates were also made by RTM with the fiberglass fabric as part of this study.

Fiber orientation will have a large effect on the flow behavior of the resin as it contacts the fiber. Permeability of the material changes as the directionality of contact is altered. This also can change the amount of tortuosity in the resin path as the different shear forces of the fibers act upon the resin. All plies for the infusion process were oriented in the 0^o orientation to simplify complexity of void movement simulation. Simulation becomes more complex as orientation of the fiber becomes more quasi-isotropic.

Reinforcement fabrics were measured and cut in 400 x 300 mm plies. Careful attention was given to ensure limited fiber strands were lost in the cutting process and transition from cutting table to mold cavity. Loss of fibers can decrease permeability and promote "race-tracking" and affect the flow of resin through the cavity. Five plies were stacked into the mold for each laminate, a number determined from the areal weight (0.518 kg/m^2), fiber density (2,550 kg/m^3), mold thickness (2 mm), and target v_F of typical vacuum infusion laminates with the same fabric (45 to 50%).

3.2.4 Resin System

Rhino 1411 epoxy resin with Rhino 4111 slow hardener was carefully measured given our calculations to determine the proper volume of resin needed. The desired volume was determined by first estimating the fiber volume in the RTM tool cavity. After this was calculated, the remaining volume of the tool cavity was determined to be resin. Volume of the one meter long hose was added to the predicted volume of resin. The density of the resin was multiplied by this volume to determine the mass of resin required for full infusion. A 100 gram buffer was added to the required resin content to ensure air was not introduced to the cavity during infusion.

The epoxy resin was mixed carefully to not introduce unwanted air into the mixture. After mixing for three minutes, the resin was placed in a vacuum chamber for five minutes to evacuate any air introduced during pour or mixture. The cup of epoxy was then placed into the infusion pressure chamber.

3.2.5 Infusion Process

Each infusion followed the same process. The tool cavity was sealed and the surrounding bolts were tightened to specifications following a provided tightening pattern. The pressure vessel connected to the RTM tool by a one meter long tube and an additional tube of random length was attached to the vent side of the tool (see figure 3-4). Pressure was then applied to the chamber and the vent hose was closed. The pressure gage was watched to verify there was no change in pressure over a one minute hold. Once the pressure system and tool passed pressurization tests, the cup of epoxy was placed into the chamber, the chamber was re-sealed, the inlet hose was clamped shut, and the vent hose was opened. Both ambient and tool temperature were recorded at this time.

Figure 3-4: RTM Tool Configuration

After the chamber was pressurized, the clamp was removed and resin allowed to flow to the tool. A stopwatch was started as soon as the resin hit the inlet of the tool and stopped once the resin reached the vent. The goal is to not vent the entrapped and formed bubbles but to hopefully trap them in place, so the pressure was immediately shut off and the inlet and outlet hoses clamped shut as soon as resin was seen in the outlet hose. The laminate was allowed to cure at room temperature for 12 hours, which was followed with a post-cure at 85^{o}C for one hour. The composite laminate was then removed from the mold and prepped for testing.

3.3 ACAB Panels Processing

Two laminates were prepared at ACAB prior to my arrival on this project. ACAB produced two laminates, referred to as "G" and "H" in this report, in an 800 x 400 x 4 mm mold cavity. They were produced by RTM from an aerospace-grade carbon fiber unidirectional weave with a powdered binder and infused with RTM-6 epoxy resin with an industrial infusion

machine. The infusion machine pre-heated the mold and resin to 180°C and maintained temperature throughout the infusion.

Each laminate was injected at a predetermined velocity (flow rate). The infusion machine was set to 100 cm^3/minute for laminate G. After half of the laminate length, or approximately 400 mm, the infusion machine reached maximum available pressure (2.25 bars gauge pressure – calibrated as the pressure above atmospheric pressure). The infusion was then continued as a constant-pressure infusion at that maximum pressure capacity of the machine. In RTM at constant pressure, the flow rate continually decreases as the flow front travels farther from the inlet, due to more of a pressure loss across the increasing size of the filled regime of the preform, the infusion machine was set to 400 cm^3/minute for laminate H, but the maximum available pressure was reached after only a few centimeters of flow, thus the majority of the laminate was filled at constant pressure with a decreasing flow rate.

The applied pressure was turned off just before completion of filling for both laminates to ensure that the resin would cure with all formed voids still in the laminate. Both laminates were cured at 160°C and allowed to cool before removal from the mold.

3.4 Sample Preparation and Laminate Layout

Each laminate was cleaned with dish detergent and water followed by a wipe with isopropyl alcohol to remove remnants of release agent. The panel was then marked per the layout in Figure 3-5. Most of the samples were taken from the section of the laminate further from the inlet as void content concentration usually is highest further from the resin inlet due to the propensity of voids to move with the pressure gradient towards the vent. Samples set for SBS testing were mapped per ASTM D2344. Given the average sample thickness of 2.67 mm calculations were performed for length and width of the sample. SBS samples measured 16.0

mm x 5.33 mm x 2.67 mm. Microscopy and combustion samples were also measured to 16.0 mm x 7.00 mm x 2.67 mm. Samples were then cut on a standard tile saw with a six-inch diamond blade. A stop was set to assist in keeping sample width consistent.

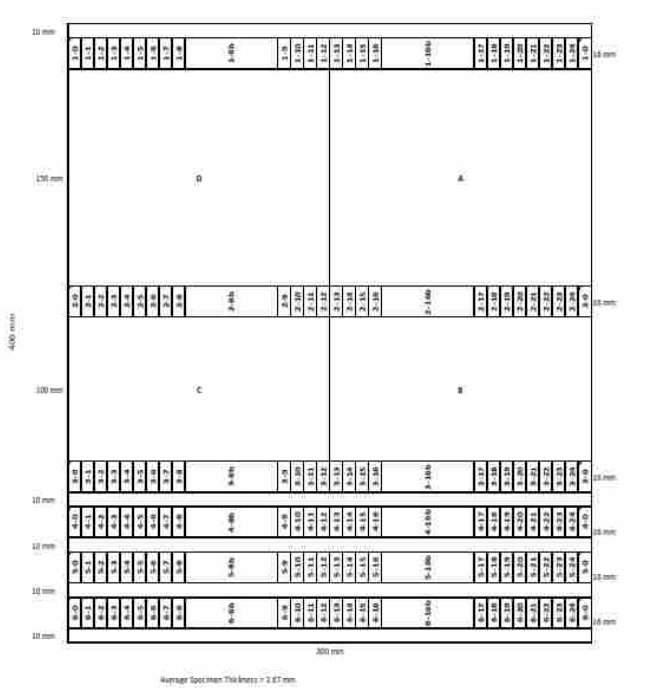

Figure 3-5: Specimen Labeling and Sectioning

3.5 Void Content Measurement

3.5.1 Macro-Lens Photography

This process was developed during the development of this thesis work. It was developed as a non-destructive test method of quick measurement of void content in transparent laminates without the need of complex, expensive equipment. A photograph was taken of a defined area on both sides of each panel with a Sony SLTA77V-a77 Digital SLR camera with a macro lens.

Backlighting was provided from a standard photography light setup located in our Industrial Design program's studio. Each image was taken in RAW and developed in Adobe Photoshop.

Images analysis of all digital images was performed using Image-J, a freeware public-domain Java-based program available on the Internet. The particle analysis tool in Image-J was utilized for its applicability to measure bubble areal coverage in a photo. This tool takes a binary image and looks for circular outlines. It then labels and catalogs each circle, measures its surface area and then calculates the image's total areal percent covered in circles. This method has been adapted by Andrew George at BYU from a process typically used for fiber count analysis.

A number of variables in Image-J are adjusted to properly focus the image including: gray-scale, shading, and brightness. The image is adjusted until the quality of the image allows recognition of bubbles without picking up other imperfections in the laminate. Image background noise from improper lighting is controlled through the particle analysis tool.
The particle analysis tool is adjusted to define limits on size of particles detected as well as define the limits on the circularity of the detected particles. A minimum circularity specification is called out to filter out long black lines in binary images created from scratches in the laminate or fiber texture patterns. The image was then sharpened to define each circular area more clearly.

3.5.2 Optical Microscopy

To measure void content, the samples were sent back to Brigham Young University to be polished and analyzed. Each sample, measuring 16.0 x 6.00 mm, was placed in a capsule and embedded in epoxy resin. After the resin cured, the disks were removed and polished using standard metallurgy sample polishing procedures. The samples were ground with decreasing abrasive diamond wheels and slurries. Each sample was initially ground with a 125-micron wheel followed by a 10-micron wheel. They were then rough polished with a 9-micron lapping

film. Afterwards, they were polished in a 0.3-micron alumina suspended in distilled water on a silk pad.

The polished samples were put under a Zeiss AxioObserver A1M microscope with a Sony SLTA77V-a77 Digital SLR attached to record images. Five images were taken along the length of the specimen and then analyzed with Image-J analysis software by computing the areal percentage of each image representing voids.

3.5.3 Combustion

The combustion process of measuring v_0 is related to Test Method II in ASTM D 3171. An approximate volume of all solids and voids is calculated by multiplying the measured thickness by the laminate's length and width. The weight of the fiber is retrieved from measurement of the weight of the dry preform before infusion. The weight of the resin is the difference between the weight of the cured laminate and the dry preform. The actual volume of all solid components (fiber and resin) is then calculated from the densities of each component. The difference between the two volumes, one with voids and the other without, is the volume of air.

3.5.4 C-Scan Attenuation

The ultrasound C-Scan measurement on the ACAB panels was performed by an operator at the Swedish Institute of Composites (SICOMP) (Operator "A") using a Sonatest RapidScan roller with a phased array (PA) transducer. The measurement was then repeated by another operator at ACAB (Operator "B") using an industry standard immersion tank, also with a PA transducer. An appropriate time-corrected gain (TCG) was determined separately by each operator, based on a nearly void-free laminate of the same thickness and fiber-resin combination.

The ultrasonic absorption coefficient α (dB/mm) is the attenuation divided by the sample thickness.

The local attenuation at the same spot on each laminate was compared to results gathered from each 16.0 x 6.00 mm microscopy sample gathered after c-scan measurement. The local attenuation was compared against each sample's macro-void and micro-void volume percentage.

3.6 Short-Beam Strength

Short-beam strength testing was performed per ASTM D 3422/D 2344M-00 at Plasan Carbon Composites on an Instron 5569A running Bluehill software. The Instron was calibrated as of April 27, 2015. The test was run with the specified loading nose and supports. Each sample that was cut from the laminate was measured to the hundredth of a millimeter with a pair of six-inch calipers. No special conditioning was performed on the samples before testing other than being stored at temperature in the testing lab.

Specimens were inserted with tool side A surface facing upward equidistant between the side supports. The specimens were then loaded at a rate of 1 mm per minute. The loading was continued until either of the following occurred: 1) a load drop-off of 30%, 2) two-piece specimen failure, or 3) the head travel exceeds the specimen nominal thickness. Data was recorded mapping the load versus crosshead displacement. The maximum load, final load and the load at any obvious discontinuities in load-displacement data were recorded.

Short-beam strength was calculated per equation 4-1.

$$F^{sbs} = 0.75 \text{ x} \frac{P_m}{b \text{ x } h} \tag{3-1}$$

Short-beam strength is related to the maximum load observed during the test, N (lbf), the measured specimen width (mm), P_m, the measured specimen width (mm), b, and measured specimen thickness (mm), h. For each series of test methods, the average short-beam strength was determined as were the standard deviation and coefficient of variation (in percent) for each property.

4 RESEARCH RESULTS AND ANALYSIS

Fiberglass infusions were carried out through the above protocol and the initial data of processing parameters was analyzed. Varying infusion times were evident not only between separate pressures values but also within infusions performed at the same pressure value. Infusions performed at 1.00 Bar ranged from 2:01 minutes in Laminate C compared to 4:13 in Laminate D (see figure 4-1). Temperatures at infusion were only separated by 0.8^{o}C, which would have little effect on change in pressure gradient or resin viscosity. The variation in pressure gradient is the applied pressure minus the atmospheric pressure on the vent. This variation does not change much over such a small difference in temperature. Previous studies have also shown that resin viscosity rarely has an effect on flow variation and may result in only a 2% increase in fill time where the variation in fill time in this sample of infusions ranged from 10-210% (George 2011). According to Darcy's Law (equation 2-1) the remaining variables in flow variation are permeability and porosity of the reinforcement.

The possibility that the resin was able to flow more quickly through the laminate could be related to the density of the fabric . The JB Martin fiberglass easily lost strands while handling which could promote race tracking and reduce areas of interference that slow resin flow. Fiber density could also lead to variation in fill time due to non-ideal packing of the reinforcement in the mold at the sample edges issuing an increase or decrease in resin flow. Another consideration for variation possibly demonstrated in this sample set could be the typical variation in

permeability of the fabric. It has been found that permeability of the same reinforcement material can vary approximately 20% from test to test (Vernet 2014). This variation simply comes from micro-variation in the fiber architecture that causes high variation in flow-rate.

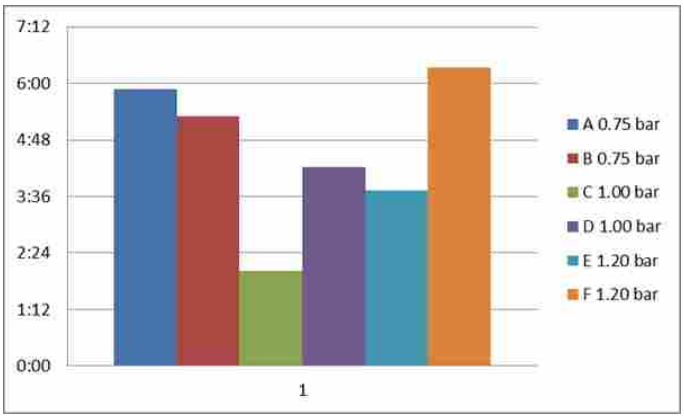

Figure 4-1: Infusion Flow-time Comparison

Traces of ink from marking the fiber for cutting were identified in Laminate D that appeared to represent the path of resin flow (see figure 4-2). It was visible that the markings flowed from the inlet-side and continued to fade towards the vent port following the expected 1D flow of resin with tracers fading towards the vent (orange dot in middle photo of figure 4-2). An interesting observation was, that despite a flow channel machined along the vent side of the preform, the tracer suggests that the flow is moving diagonally towards the actual vent port instead of uni-directionally towards the vent channel. The vent channel may have been too full of fibers to operate its intended function of ensuring linear flow. This suggests that the assumption of linear flow is invalid for these infusions and that void formation and flow modeling will be more complex than simple one-dimensional flow. The ability to track resin flow in a closed, metal tool has not been accomplished yet and this observation provided a possible method of

tracking such flow. After noticing this phenomenon, tracers of different markers, permanent (same type used to mark dry fabric) and dry-erase markers were used to map a dot pattern on Laminate A to possibly provide evidence of flow path through the laminate. The results were inconclusive (flow path traces were not detectable) but research into other tracer materials would be a valuable path to evaluate in the future to assist in the mapping of flow in a closed-mold tool. In this instance tracers would have provided clarification on whether and where race-tracking or a lag in flow rate occurred.

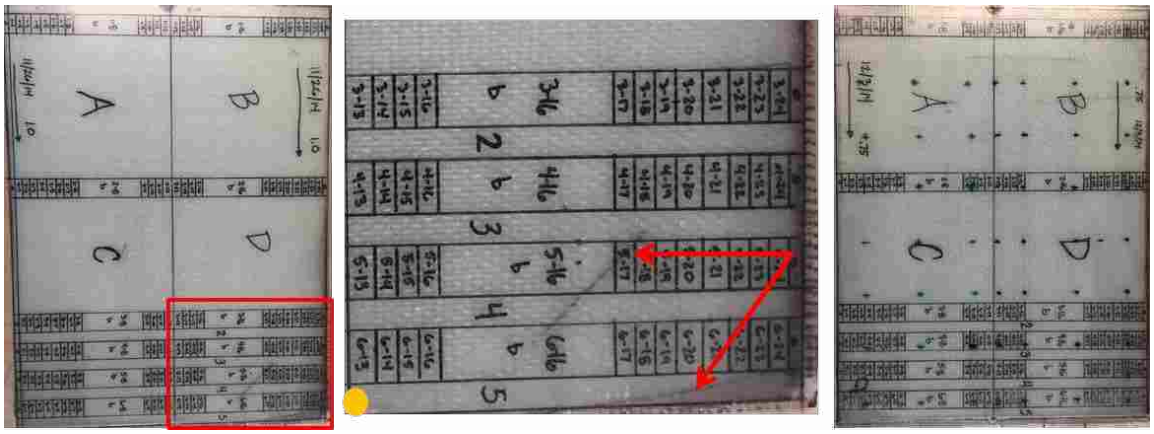

Figure 4-2: Trace Markers in Laminate. Initial Observation of "Tracers" (Left) and Highlighted (Middle). Attempt to Replicate with Mapped Dot Pattern (Right).

4.1 Void Measurement

4.1.1 Macro-Lens Photography

The carbon laminates made by ACAB were not analyzable by macro-lens photography due to the opaque nature of the carbon fibers. Each fiberglass sample, however, was initially photographed for v_0 measurement through macro-lens photography void characterizations. In a

previous paper this method was developed and determined to offer comparable results between density/thickness measurements when compared to macro-lens photography samples of transparent materials such as glass fibers (George 2013). In this situation, however, either the higher fiber content or the fiber architecture was promoting excess levels of noise in the photo, with many of the rovings appearing as black lines. The frequency of such lines greatly convoluted the appearance of the bubbles; rendering particle analysis results obsolete (Figure 4-3). It was difficult to highlight the laminate with the proper lighting that would allow site of voids in the laminate, which in turn could be analyzed through the algorithm in Image-J software to determine v_0 throughout the laminate. These measurements were unable to be performed on these laminates.

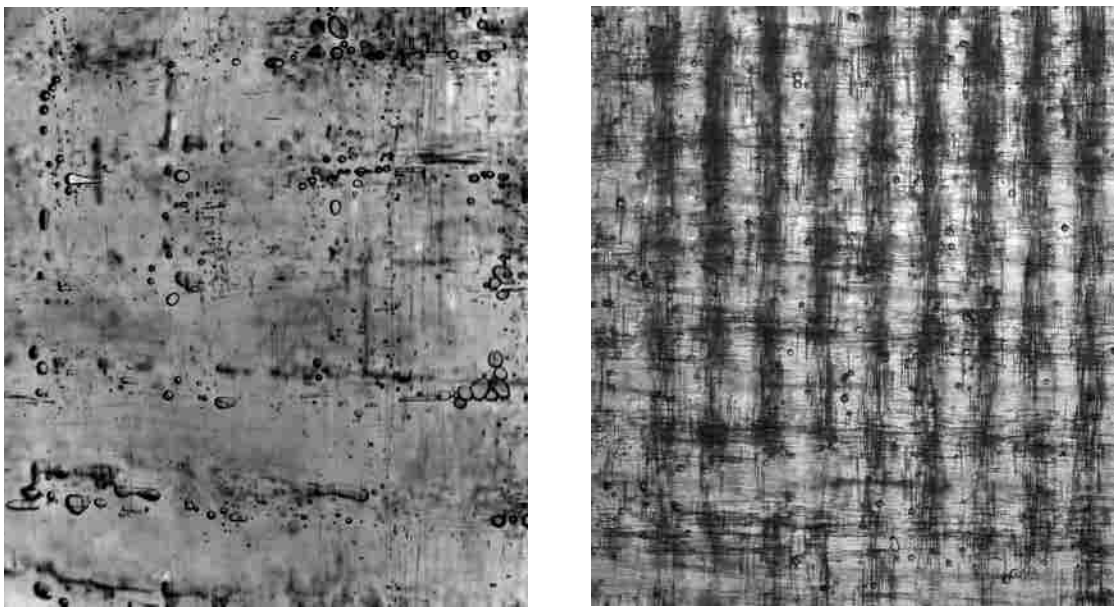

Figure 4-3: Macro-lens Photograph Successfully Analyzed in (George 2013) (Left) and of Fiberglass Laminates in this Study (Right).

4.1.2 Optical Microscopy

For the carbon laminates G and H, sample polishing and microscopy was performed by SICOMP. Three micrographs were imaged of each sample cut from various locations in each laminate. The micrographs were then analyzed at BYU in Image-J; the areal percent of macro-voids and micro-voids was separately calculated for each image (figure 4-4)

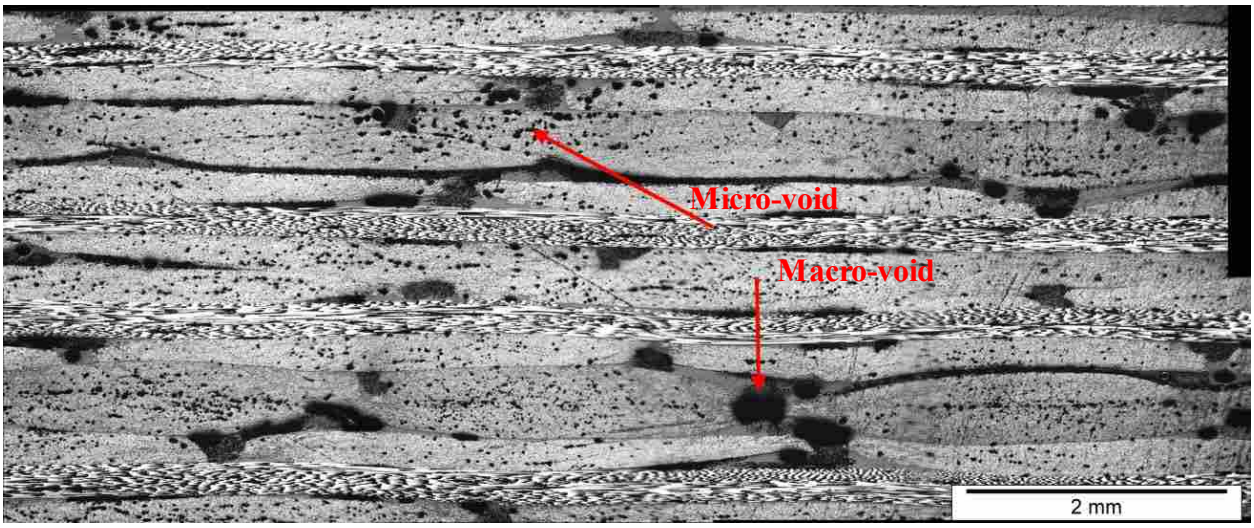

Figure 4-4: Example Micrograph from Laminate H Showing Both High Micro-void and Macro-void Content.

For the fiberglass laminates A-F in this research project, void content was measured by optical microscopy for all samples. But only macro-void contents were measured, as micro-voids were too difficult to discern from polishing artifacts in several of the images. Figure 4-5 illustrates examples of fairly good polishing, in which both the macro-voids and micro-voids are evident, as well as an example micrograph where the polishing was not sufficiently high quality to measure micro-voids. Unfortunately, the majority of images were more like the latter than the former, so micro-void content measurement for this sample set will have to wait until future work can be done to improve polishing methods for these samples. Micro-void measurement,

such as that done with the ACAB carbon laminates (G, H) remains a difficult task in all void measurement methods due to their small size.

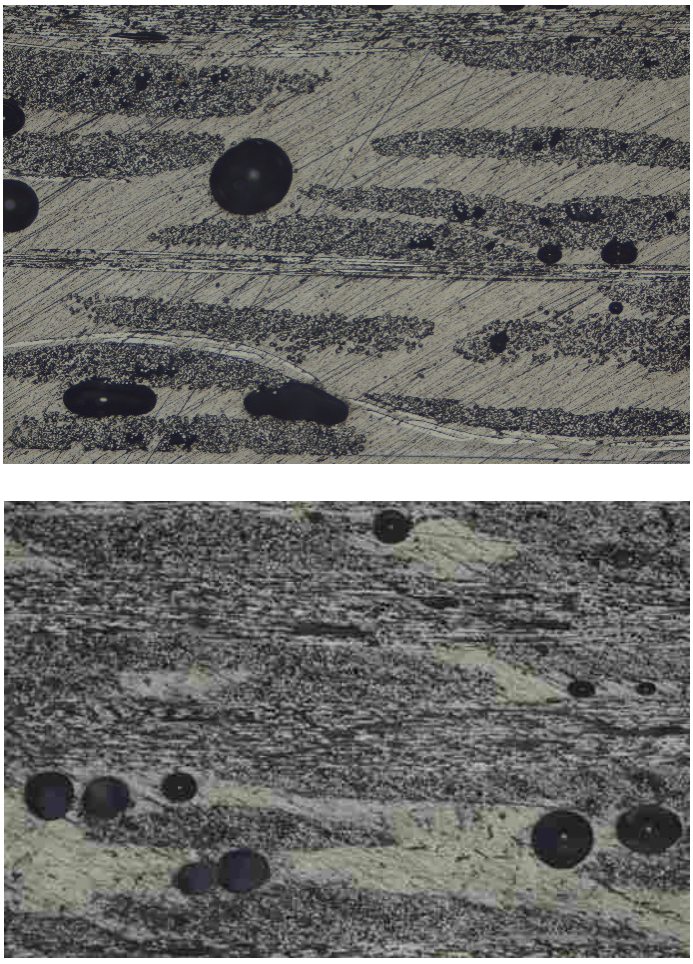

Figure 4-5: Sample Micrographs from Fiberglass Laminates: High-Quality Polishing (Top) and Low Quality Polishing (Bottom)

The data for the laminates G and H provided strong correlation with expected results per dual-scale flow theories. Areas under higher pressure with faster flow rate (close to the inlet) showed little porosity primarily consisting of micro-voids. As the flow front moved away from the inlet and the flow rate decreased, the introduction and growth of macro-void presence increased. Sample row 3 of laminate G contains less than 1.00% overall v_0 with 0.81% v_{0M} and

jumps to 2.00% overall v_0 and 1.56% v_{0M} in the neighboring sample set in row 4. This trend continues in laminate H but with the steady increase in v_0 beginning in row 5. The further from the inlet the resin flows, the lower the flow rate and higher void content.

Microscopy results for the fiberglass laminates did not show as drastic of a differentiation in void content as the flow front moved along the length of the panel (see figure 4-6). The difference of void content along the flow path is not as clear, even though a slightly lower porosity by the inlet is seen compared to by the vent. Averaging the v_{0M} of each laminates rows for both the ACAB carbon fiber laminates (orange) and fiberglass laminates (blue) showed a definitive change along the laminate in the ACAB panels and a much slighter trend in the fiberglass. Rows 3 and 4 peak the amount of v_{0M} and then it begins to slightly trail down. It is speculated that with the more porous material with wider tow gaps, the macro-bubbles not completely entrapped were able to escape through the flow front.

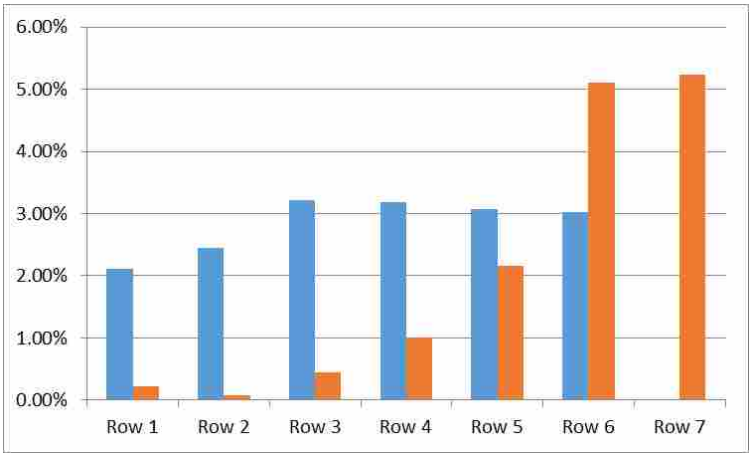

Figure 4-6: Comparison of v_{0M} Between ACAB Carbon (Orange) and Fiberglass (Blue).

Not only does the void content differ between the two reinforcement types, but the appearance and shape of the voids vary. The ACAB panels' tightly packed architecture have no

circular voids as seen in the "looser" fiberglass samples (figure 4-5). The ACAB panels display voids that are deformed by this tight reinforcement packing that tend to be long, thin macro-voids between plies and small in comparison to tow size. The fiberglass reinforcement was not as tightly packed and had less compaction of air bubbles, allowing them to appear more circular and large compared to roving size.

4.1.3 Microscopy and Combustion Comparison

Void measurement via combustion were completed on laminates A and E and compared to the results found through microscopy void measurement. The results are found in figure 4-7 where a comparison for each panel, its row and the process of measurement is compared. It is clear that there are large discrepancies between the two measurements but the microscopy method only measured the volume of macro-voids, whereas the combustion samples measured both macro- and micro-voids. Therefore, measured void content will be higher.

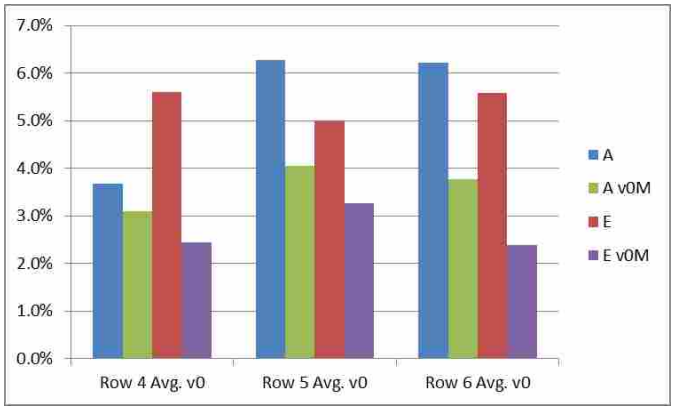

Figure 4-7: Combustion v_0 (Blue and Red Columns) vs. Microscopy v_{0M} (Green and Purple Columns) for Select Samples Close to the Vent from Laminates A and E.

It is difficult to determine how accurate each method is to one another without a true analysis of micro-voids. Simply re-polishing the microscopy samples could yield clearer samples where micro-voids can be read and included in prediction of overall void content. Both processes have their weaknesses and strengths. The combustion process is typically only used on glass substrates since it leaves a residue on carbon substrates which then interfere with weight measurements. Combustion sampling provides a void measurement of a sample throughout its volume whereas microscopy predicts what the through-volume void content is by analyzing one side. Microscopy yields quicker results than the tedious process of combustion and provides more useful information though including: void location, shape, and distribution within a sample.

4.1.4 Ultrasound and Microscopy Correlation

Initial ultrasound measurements were performed on Laminate G and Laminate H. These ultrasound measurements had already been taken on these laminates at ACAB and the attenuation data was used as a comparison to measurements taken on a similar unit at SICOMP. Re-measurement was carried through to 1) provide data for verification of NDT equipment and 2) validate repeatability of such test methods. Data analysis and comparison of ultrasound results was performed at Brigham Young University (BYU).

Figure 4-8 displays Laminate G as well as its c-scans by both operators. It is clear to see a large area of low porosity covering the top half (by the inlet) of the laminate, that begins to transform into a strip of high attenuation as the scans approached the flow front. The local attenuation of each microscopy sample was extracted from the c-scans and compared against the samples macro-void (v_{0M}) and micro-void (v_{0m}) measurements determined from optical microscopy testing. These results are shown in figure 4-9, which displays a roughly linear increasing trend in ultrasound attenuation with increasing macro-void concentration.

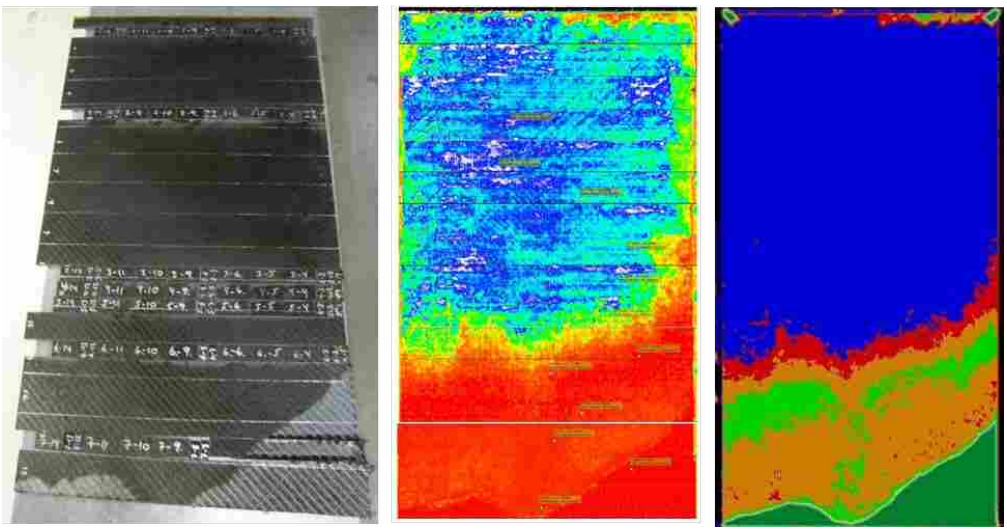

Figure 4-8: C-scans of laminate G by SICOMP (Middle) and ACAB (Right).

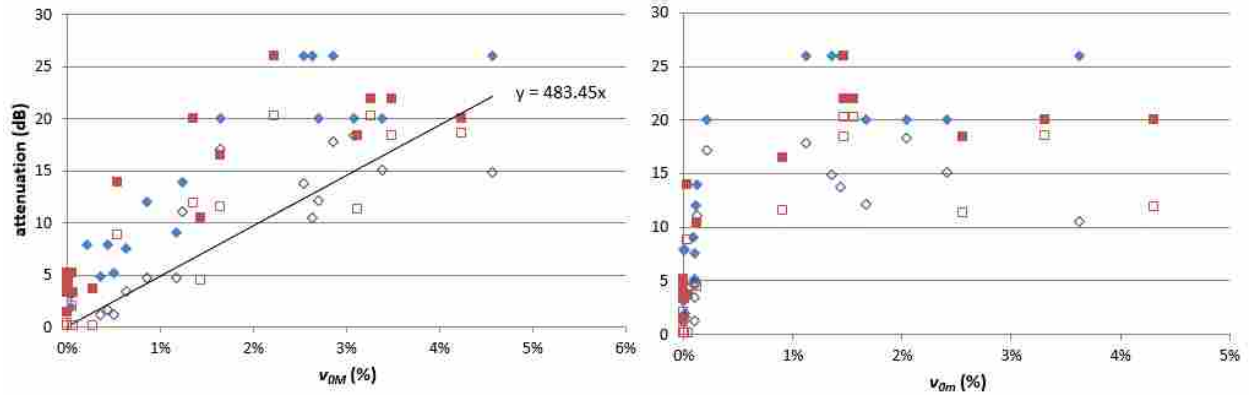

Figure 4-9: Local Macro-void (Left) and Micro-void (Right) v_0 vs. C-scan Attenuation for Laminates G (Blue) and H (Red), as well as for SICOMP Measurements (Solid Symbols) and ACAB Measurement (Hollow Symbols).

The graph of percent micro-void content compared to attenuation surprisingly lacked correlation with rising attenuation. There are no micro-voids in the low attenuation sections and the areas with micro-voids produce no reasonable correlation. Considering that c-scan resolution is in the order of size of micro-voids, it suggests that all attenuation is being provided from the presence of macro-voids and the equipment struggles to notice micro-voids. The comparison of

micro-voids simply shifts points to the right with growing v_{0m} without adding attenuation. A direct comparison of micro-voids to macro-voids was not able to be performed since no samples contained a significant reading of micro-voids along with no macro-voids, i.e. any sample with micro-voids also contained a significant amount of macro-voids (e.g. Figure 4-4). Without samples like these, it is not probable to determine what attenuation reading is only caused by micro-voids. This implies that the correlation in figure 4-9 would be convoluted if attenuation was correlated to the entire panel's overall void content (both micro- and macro-) as is typically done. If micro-voids do not produce further attenuation, then c-scan correlation should be only compared to macro-void content.

Variation between attenuation data collected at ACAB versus the data collected at SICOMP is most likely attributed to the particular TCG sizing chosen by each. A linear trend line represented in macro-void versus c-scan attenuation graphed on the left of figure 4-9 corresponds to laminate G as measured at ACAB. The resultant attenuation in micro-void c-scan measurements shows an increased range without any measured micro-voids followed by a wide range of attenuation for the different concentrations of measured micro-voids. This is suspected to be in part of the limitations of resolution in c-scan equipment, where the ultrasound wavelengths are too large to pick up the micro-voids in a composite laminate.

A relationship between c-scan attenuation and macro-void volume percent in the fiberglass panels was not as straightforward as the carbon fiber data. The c-scan attenuation shows a checkerboard pattern of high variation in attenuation. This is attributed to the fiber architecture where its fabric pattern caused a change in attenuation during scanning. This complicated the data by giving a general range of 30-50% attenuation across the surface area

(see figure 4-10). This high local variation in attenuation would lead to a high variation in prediction of local void content in the specified area.

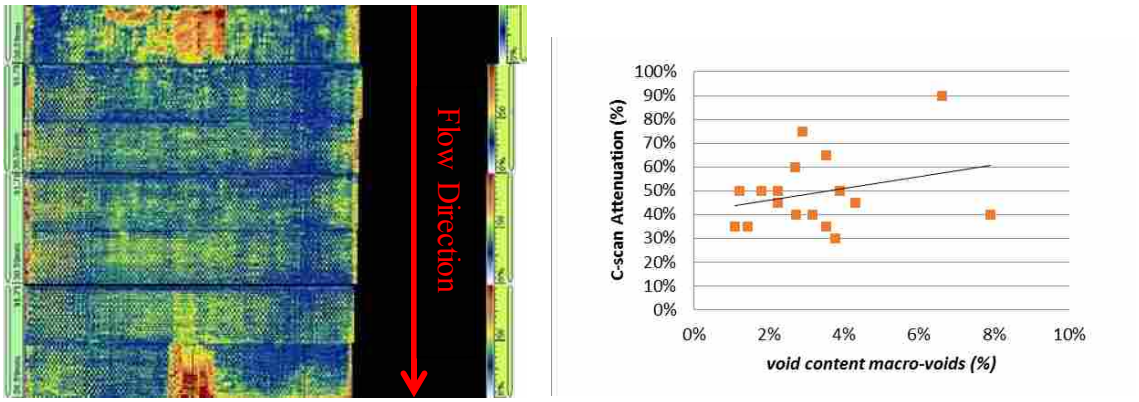

Figure 4-10: Laminate D C-scan Attenuation Compared to Macro-void Content Measured by Optical Microscopy.

In order to collect data on c-scan attenuation for the fiberglass laminates each panel was overlaid with a transparent map of the sample labeling and sectioning scheme to match up the c-scan to location of samples. From here each sample was highlighted with a box. This allowed one to look at the area and subjectively choose a percent attenuation. There is a lot of discrepancy here which leads to uncertainty in the data where a sample's percent attenuation does not correlate well with measured v_0 from both combustion and microscopy. Some samples show large amounts of attenuation but only 1% v_0, which high attenuation should signal higher void content. This lack of a clear correlation between c-scan attenuation and void content was noticed through all of the fiberglass panels. When graphed, the other laminates showed almost no slope in linear fits to the data, or the slope was slightly negative, implying an error in the measurement method.

Laminate D did show that as void content of macro-voids in the sample increased, so did the c-scan attenuation. The linear trend line displayed in the graph of figure 4-10 displays a roughly linearly increasing trend in the data and given more data points could more strongly represent this relationship. This relationship is not as prevalent as the carbon fiber samples, but it does continue to validate the effectiveness of c-scan attenuation to determine a quick, NDT value of void content in a sample.

4.2 Void Formation, Movement and Dispersion

Modeling of void formation was performed on the carbon fiber samples from an end result working backwards method rather than attempting to simulate void formation during infusion. This is an inverse-estimation method (IEM) similar to that previously used in permeability fitting (George 2011). This void modeling method includes fitting the relationship between flow rate and micro-/macro-void formation to void movement and dispersion models as well as the final void distribution data measured through experiment. In other words, the process used here was to conjecture at models for these relationships and compare our prediction to our actual measurements of final voids while iterating the void formation models until they approximate the true final void content. Such modeling has only been thus-far attempted with the carbon laminates made by ACAB as more information concerning both macro- and micro-void contents was available. In these laminates, voids were purposefully left in the final laminate by stopping the infusion before the flow front reached the vent. This allowed the bubbles that were in the resin to become trapped as voids. Micro-voids and macro-voids are analyzed separately.

4.2.1 Micro-void Formation and Dispersion

Predicting micro-bubble formation required evaluating a number of variables that are present during the infusion and comparing the resultant characteristics of the laminate to models predicting formation and dispersion. Recent publications on void prediction tend to model bubble formation as a volumetric percentage of the composite material which is a linear function of the natural log of the modified capillary number (see equation 4-1) (LeBel 2014, Gueroult 2012).

$$v_0(\%) = A \ln\left(\frac{\mu v}{\gamma cos\theta}\right) + B \tag{4-1}$$

In this equation, the capillary number is determined by the formula contained in the parentheses. The resin's viscosity, μ, flow velocity, v, surface tension, γ, and contact angle, θ predict the capillary number. A and B are fitting constants for the bubble formation model. Previous findings, both unpublished work at SICOMP and published works, were used to determine the surface tension of epoxy, the contact angle of epoxy on carbon fibers, and resin viscosity for RTM-6 over time and temperature. The flow velocity was determined from the infusion equipment at ACAB, measuring the infusion flow rate every 2 seconds.

Figure 4-11 displays data gathered from laminate G which was infused at 100 cm^3/min. The orange dots represent the v_{0m} measured through optical microscopy for each sample along the length of the infused panel. Through evaluation of this dispersion, the only area showing any considerable micro-void concentration was the last 20% of the laminate length along the flow path. The final pressure gradient representing the length of the infusion from inlet to flow front is represented by the red line and the left axis. This displays the resin pressure gradient at the moment before the over-pressure was shut-off and the mold was vented to atmospheric pressure.

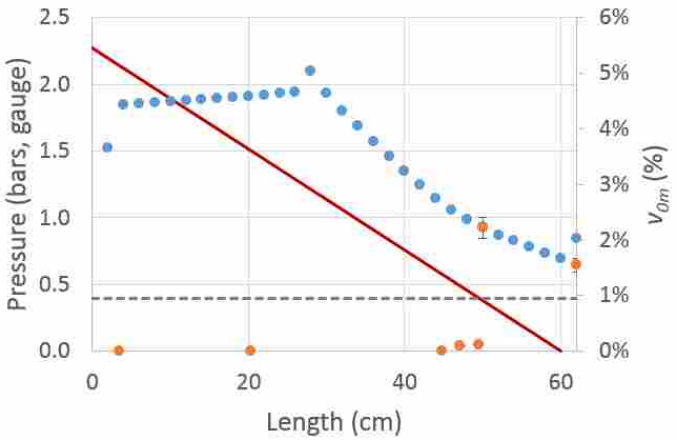

Figure 4-11: Micro-void Formations and Modeling: Final Pressure Gradient (Red Line) Across Filled Regime's Length Just Before Shut-off of Over-Pressure. Cured Part's v_{0m} (Orange Dots) by Position Along Filled Regime, as Well as Predicted Formation of v_{0m} (Blue Dots) by Position. Gray Dotted Line Represents Pressure Threshold for Complete Diffusion of Micro-Bubbles.

This reveals a 10-17 cm zone at the end of the laminate where the only micro-voids are apparent in the cured laminate. An assumption is made at this point. Lundstrom predicts in his paper, "Measurement of void collapse during transfer moulding", that the dominant mechanism for change in intra-tow micro-voids has been proven to be diffusion (1997). Through Henry's Law, as the pressure in a fluid is increased, more gas is able to dissolve into a fluid. In the case of an infusion, the applied pressure is acting on the bubbles that are not able to escape through the flow front. Bubbles will continue to shrink, per the ideal gas law, and disappear into the resin solution. The large pressure acting on the laminate near the inlet is why few micro-voids are found near this point in RTM infusions. The fiber architecture of the NCF carbon fiber contains fiber tows that are so tightly packed it is predicted that micro-voids are not able to escape and become entrapped where they are formed as the flow front passes that location (Lundstrom 2010).

This leaves the only remaining mechanism for micro-void dispersion after formation – diffusion. From here it is assumed that there is a pressure threshold where all micro-voids will

dissolve. When looking at the graphed location of micro-voids and related to the pressure where they begin to be seen, we are able to predict that micro-voids will be dissolved into solution at pressures above 0.4 bar. This pressure threshold is represented in figure 4-11 as the grey dashed line. It is therefore assumed that all micro-voids at a higher pressure then the threshold will dissolve into the resin. Only after the pressure drops below this point will micro-voids begin to appear.

If we assume that none of the micro-voids move after formation and the remaining dissolve at the threshold pressure of 0.4 bars, then we can fit the micro-void formation curve (blue dots in figure 4-11) to the experimental (orange dots) for the last two locations. Guess values for the two fitting variables, A and B, were taken from a similar model fitted to experimental infusions done with unidirectional fiberglass infused with silicone oil and applied to the same model as in equation 4-1. Surprisingly, the fitted model from the glass and silicone oil agreed well with the two experimental data points in this study for a UD weave of carbon fiber and RTM-6 without any further fitting iterations. The fitted constants used are $A = 2.9$ and $B = 21.8$.

This model allows for change in viscosity over time which is demonstrated in the slow climb in predicted micro-void formation over the first ~40% of the flow length. There also appears to be an inflection point at ~280 mm where the infusion machine reached its maximum allowable pressure. The flow rate continued to drop from this point on, thus decreasing the predicted micro-void formation by equation 4-1.

According to the model a large amount of micro-voids were formed during infusion, but only few remained entrapped in the resin. This implies that all of these air bubbles are diffused into molecules and dissolved in the resin. An assumption is made that the small diffused

molecules of air constituents continue to travel with the flow of the resin and only become detectable once pressure drops below the threshold. In this case, this would occur once the mold was vented when infusion was cut-off.

The void formation models that were used in this research showed strong correlation with actual micro-void formation. The model represents that all voids formed but does not show what happens to the voids after formation. It has been determined that the majority of these micro-voids are dissolved as pressures above the threshold are reached. As the pressure decreases other dissolved micro-voids traveling along the flow front will come out of solution. It is assumed that these come out as nano-voids that are unable to be measured with standard microscopy procedures. Further research will need to be done to determine whether these nano-voids have any effect on mechanical characteristics.

It can be concluded that micro-void formation follows the model developed by Breard but that model only considers the formation of such voids. It does not predict what becomes of them and whether or not they will remain in the laminate or if they will escape or dissolve as seen in these trials. This model will need to be coupled with pressure threshold predictions in order to fully predict void behavior.

4.2.2 Macro-void Formation and Dispersion

According to previous work, macro-voids form a bell-curve distribution based on size in part to the variation in inter-bundle gap sizes (Frishfelds 2008). Smaller macro-voids formed in larger inter-tow gaps tend to move along with the flow front and escape while larger voids become trapped and form a cylindrical shape, similar to those seen in Figure 4-4. These voids are held in place due to the drag forces from the surrounding fibers (Lundstrom 2010). As the pressure gradient behind them continues to increase, they too are affected by the Ideal Gas Law

and begin to shrink until the threshold pressure is reached and they are able to escape or split (Frishfelds, 2008). This phenomenon was witnessed in the permeability infusions performed where visible bubbles were trapped either between tows or by stitching and gradually they would either begin to shrink or split and then race to the flow front and be evacuated in the air.

Figure 4-6 demonstrates the measured v_{0M} (orange dots) compared to the model of macro-void formation along the length of the infusion (blue dots). With the assumption that since the fitted parameters to tests using silicone oil and fiberglass used for micro-void formation agreed so well to this study, that study's results for fitting the macro-void formation model would be a reasonable guess to apply here as well. The fitted parameters for macro-void formation from that study were A = -4.9 and B = -28.1. Review of the graph below shows that little to no macro-voids are predicted to have been formed along the first half of the infusion due to the high flow velocity which would preferentially form micro-voids instead. No macro-voids were experimentally observed in samples from that first half of the laminate (orange dots). After the maximum machine pressure is reached, the flow slows down and the predicted macro-void formation increases (blue dots) at about 30 cm flow-length. But significantly less macro-voids than predicted to be formed were observed at sample locations in those areas close to the vent, implying that the pressure threshold was great enough to dissolve many of the bubbles or shrink them to a size that could easily escape. The difference between the orange and blue plots are the macro-voids that were small enough to escape. The macro-voids that were too large to escape, and have not shrunk enough to achieve mobility at the end of the infusion, are the macro-voids seen in the orange plot.

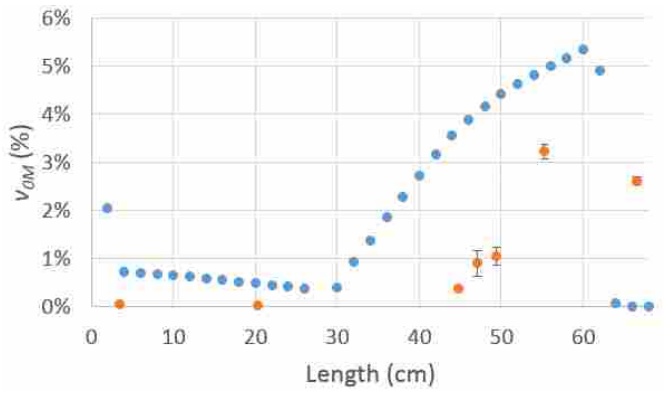

Figure 4-12: Macro-void Formation Modeling: Cured Part's v_{0M} (Orange Dots by Position Along Filled Regime, as Well as Predicted v_{0M} (Blue Dots) by Position.

In summary, the rate of macro-void formation appears to increase as the overall pressure and flow rate decrease across the laminate. Bubbles of all sizes continue to form but the amount of pressure available to shrink the bubbles to a critical size is also decreasing. It is possible that if the pressure gradient was such that it remained high enough to compress voids that over time the laminate would reach equilibrium and all bubbles would be dissolved into solution. This would require another set of tests that could be performed in the future. As seen through the test, the predicted macro-void formation far exceeds the measured void content but the model shows strong correlation to actual macro-void formation, especially when coupled with void mobility models. This could be attributed to the continuous pressure acting on the macro-voids formed behind the flow front that is able to shrink the bubbles to critical size and allow them to move quickly between the tows towards the flow front and escape. Breard's model shows strong correlation of void formation when coupled with void mobility theory. Overall void formation when coupled with an optimal flow velocity as displayed in figure 2-2 could be irrelevant if pressure threshold is considered and enough pressure is available to minimize voids. This, however, could become counterintuitive as higher pressure systems come at an increased cost, leaving lower cost processing still in need of an optimized flow rate.

4.3 Mechanical Characteristics

Previous literature correlating mechanical properties with local void content have mostly been performed with prepreg materials. As mentioned previously, these materials and autoclave processing cure under homogenous applied pressure. These mechanical properties are more easily predicted when the panel has a homogenous void content. It is hoped that a given local void content can produce the same mechanical properties in a laminate produced with the same resin and reinforcement whether it is made from prepreg or not. The difficulty in providing this ability in RI applications is the variation in local pressures and complexity of the different materials being used.

As opposed to prepreg processing, RI produces parts that are non-homogenous given the pressure gradient within the mold. Therefore, it is not possible to look at the v_0 of a panel as a whole. Void content will vary as distance and location from the infusion point changes. Instead of a holistic approach to mechanical properties of a RI laminate, one needs to section the panel and test at different lengths throughout the volume of the laminate. Each of these samples will vary and contain increased void density while others will have lower local void densities.

The testing of the carbon panels was run by SICOMP following ILSS DIN 2563. The results were averaged across each row (taken perpendicular to flow direction). By taking the samples from a perpendicular row, it is assumed that homogeneity remain constant across all samples at a given distance from the inlet in one-dimensional flow. In other words, for 1D flow testing, the local flow rate should be the same anywhere in the y-direction for a given x-direction flow length. A uniform flow across both the x- and y-directions did not occur in these laminates and the panels did not have perfectly homogenous flow. Observations of the c-scan and cured laminate clearly depict this as the resin flow front is seen lagging on the rights side of the panel

(see figure 4-13). This could be owing to micro-textile variation or irregular binder concentrations.

Figure 4-13: Lagging Flow Front

As each row's samples were observed, it could be suspected that non-linear flow fronts would provide different void formation amounts along a row of samples. Samples from the slower-flow right side of the panel were thus analyzed separately and then the remaining samples in each row were grouped together. Separating these two flow fronts provided a much clearer correlation of ILSS versus void content (see figure 4-14). The graph on the left depicts the correlation of this data before separation of samples (all samples in each row averaged together) for laminate G while the right demonstrates a clearer trend for laminate G (blue dots) when separating the slower flow samples from the other samples in each row. Figure 4-14 also shows the effect of variation in flow velocity. The data for laminate H ILSS vs. void content is depicted in red on the right graph.

There is a quick decrease in properties after the first 1-2% of voids. Laminate H showed higher levels of ILSS before failure which could be due to the higher infusion flow rate. Laminate H depicts increased areas of lower void content as well. It is suspected that the higher flow rates implemented in Laminate H should produce increased volumes of micro-voids than macro-voids per the dual-scale models illustrated in figure 2-2.

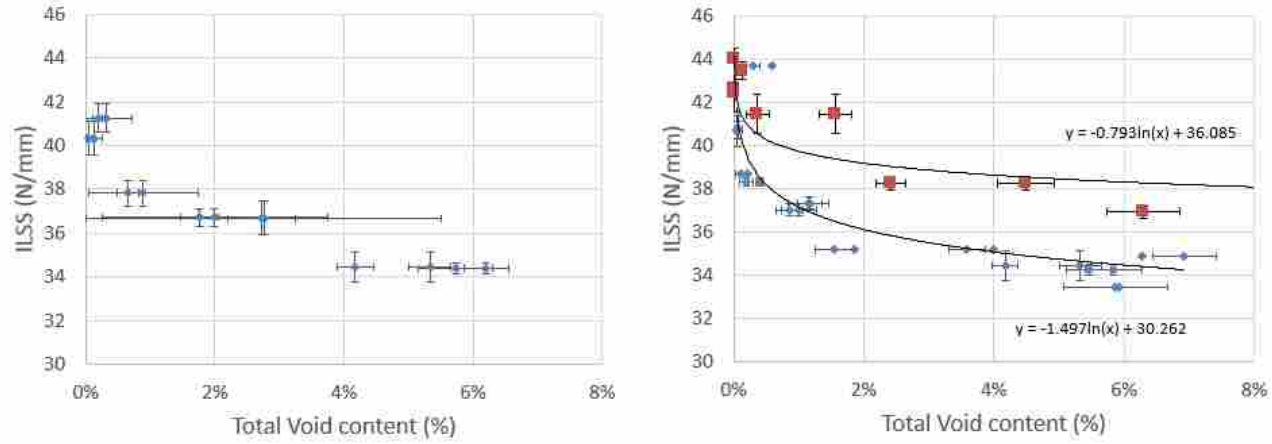

Figure 4-14: Local Measured Void Content (Total) vs. ILSS for Laminate A (Blue), Averaged Across Rows (Left) and Further Split into Groups by Location in the Rows (Right). Right-side Graph Also Displays Data for Laminate B (Red).

It is predicted that mechanical performance can be increased by simply injecting at a higher flow rate rather than constraining a process to an optimal flow rate to minimize the combination of micro- and macro-voids. The higher flow rate would then create the large volumes of micro-voids that are thought to contribute less to mechanical failure. Yet-unpublished results by colleagues suggest that fatigue is more sensitive to macro-void content than micro-void content. It is suspected that small voids within a sample are not sufficiently large to cause crack-initiation or propagation (Sisodia 2014). When comparing the ILSS to v_0, similar curves were evident for both macro- and micro-void percentage, but the ILSS sample in this case

is compared to a sample that has both macro- and micro-voids, so there is no way to determine from these results which type of void is contributing to the loss in ILSS. Future studies must focus on imaging of actual crack imitation and propagation to clarify the effects of voids of differing size and location (Sisodia 2014).

When the same principles were applied to the fiberglass infusions, the results were not as conclusive. Comparisons of SBS results as a whole from one panel to another showed little to no differentiation in SBS at different infusion pressures (see figure 4-15). Laminate C showed less attenuation in ultrasound scans than the other laminates, and had almost the second lowest macro-void content but displayed a peculiar peak in SBS in Row 5. The void content in Row 5 of laminate C is slightly greater than Row 5 of laminate E yet demonstrated a higher SBS measurement. In order to determine why this result is seen in the data, void morphology was analyzed to determine if this factor may be related to the mechanical performance of a laminate.

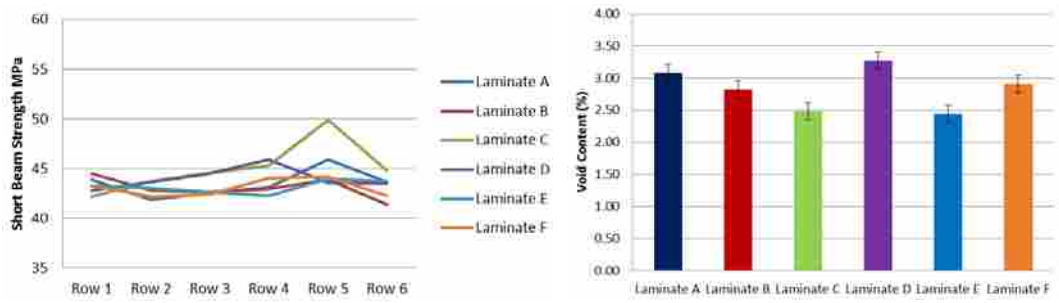

Figure 4-15: SBS Results (Left) and Average Macro-void v_0 of Each Laminate (Right).

Void micro-photographs were analyzed in a model developed by Fullwood (Fullwood 2013) that measures the length and height of each void, its area, and then produces a metric that determines an average distance between voids, termed "nearest-neighbor distance." This data was only collected on macro-void morphology and distance from one another. When the two

laminates were compared together there was little difference noticed between these metrics. The increase in SBS results for Row 5 in laminate C suggested some difference in void distribution or morphology due to the little variation in void content. Row 5 laminate C displayed a further distance to its nearest-neighbor with an average distance of 0.91 mm versus laminate E's distance of 0.80 mm (see figure 4-16). When graphed together, an apparent upward trend in SBS is seen as distance between voids increases. This can be attributed to an increased force needed for a crack to propagate to the nearest weak area or void. The cause for the larger spacing between voids in Row 5 laminate C compared to laminate E is unknown. There was also a slight correlation that displayed an increase in SBS with increasing sphericity of the voids but the profile only yielded a very slightly increasing slope. Further accumulation of data would be required to verify this relationship between effects of voids and void shape.

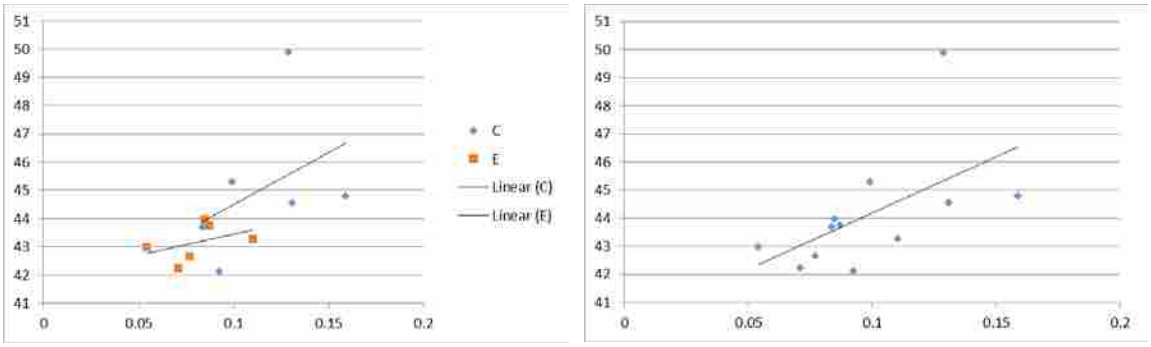

Figure 4-16: SBS Results (MPa) vs. Nearest-Neighbor Distance (mm) Compared Between Laminate C (Blue Diamonds) and Laminate E (Orange Squares) with a Linear Fit of Each (Left) and Overall Correlation (Both Laminate C and E) of SBS vs. Nearest-Neighbor Distance (Right).

In order to verify the effects of v_0 on the mechanical properties a direct comparison is needed. This comparison was performed on the middle samples taken from each laminate (A-F) and graphed in a similar manner that the laminates G and H were (see figure 4-16). This graph shows a slight decrease in SBS as v_0 increased but not as drastically as represented in the

laminates G and H. The lower clarity in the exponential trend could be due to the lack of samples with v_0 greater than 0% but less than 1%. Potentially if there were samples of the same material, dimensions and processing methods but with lower v_0 there would be a more straightforward relationship as predicted and seen previously. It can be concluded that strength is not well correlated to void content above 2% and could possibly be related to void morphology. It is difficult to fit a curve when the error bars are all over the graph width as represented in figure 4-16, which demonstrates the difficulties of optical void measurement, to represent an entire sample when only one surface of the volume is measured. And the error may be lower once micro-voids are included in the results as were done for the carbon laminates.

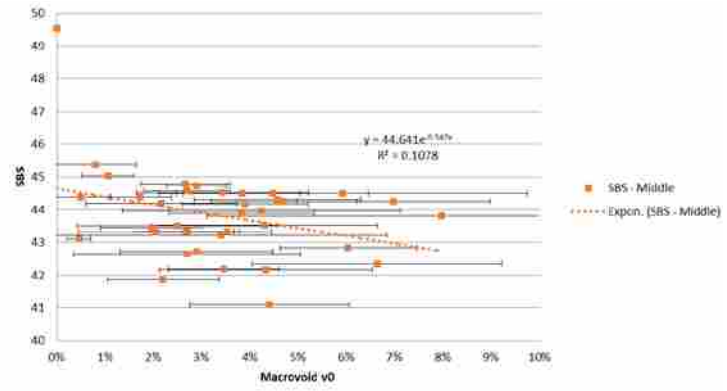

Figure 4-17: SBS vs. v_{0M} Microscopy; Error Bars Represent Standard Deviation Across Photos of that Sample. Trend Line is Linear Fit of All Data.

Each method of void measurement has determined a different void content in the end. Comparing the trends of macro-void measurement via microscopy versus SBS shows a slightly declining trend; as void content increases, SBS decreases (see figure 4-17). In contrast, when comparing percent attenuation from c-scan measurements, SBS shows a slightly increasing trend. The accuracy of void measurement and local attenuation measurement plays a significant

role in the refinement of comparisons between mechanical properties and void location and percent. It is predicted that with more time and better polished microscopy samples where a micro-void measurement could be taken, a more defined trend would appear and correlate more closely with hypothesized relationships between void content and SBS.

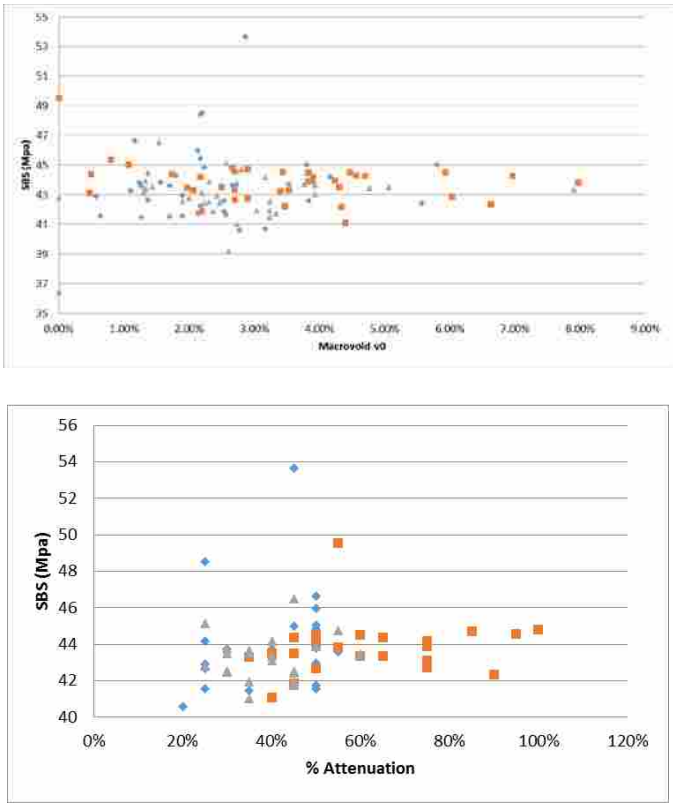

Figure 4-18: SBS vs. v_{0M} (top): SBS of Left-side Samples (Blue Dots), SBS of Middle Samples (Orange Squares) and SBS Right-side Samples (Green Triangles). C-scan Attenuation vs. SBS Laminates C-F (Right): SBS Left-side Samples (Blue Diamonds), SBS Middle Samples (Orange Squares) and SBS Right-side (Grey Triangles).

5 CONCLUSIONS

As composite materials become more and more prevalent in today's world, the ability to process them cheaper and faster while maintaining their key strength characteristics becomes increasingly important. The lack of understanding to predict the cured-in-place void distribution and the void content's effects on the mechanical properties in a resin infused laminate is a major drawback in the realization of industry adopting resin infusion (RI) processing.

An understanding of the effects of defects in prepreg composite laminates has already been studied and enabled the application of composite materials in a number of industries. With a push in automotive to produce lighter, more efficient vehicles, RI processes provide a path to reduce cost in composite processing while achieving great strength-to-weight benefits. Therefore, the demand for tools to model and predict the mechanical characteristics of a RI laminate continues to increase.

The purpose of this research is to understand the effect of processing conditions on the concentration, location and distribution of voids in a resin transfer molding composite laminate as well as the influence of those voids on the resulting mechanical properties.

5.1 Void Measurement

5.1.1 Microscopy

The void content and dispersion differs between the two reinforcement types as well as the appearance and shape of the voids varies through microscopy analysis. The ACAB panels' tightly packed architecture contains no circular voids as seen in the "looser" fiberglass samples (figure 4-5). The ACAB panels display voids that are deformed by this tight reinforcement packing that tend to be long, thin macro-voids between plies and small in comparison to tow size. The fiberglass reinforcement was not as tightly packed and had less compaction of air bubbles, allowing them to appear more circular and large compared to roving size.

5.1.2 Combustion and Microscopy Correlation

It is difficult to determine how accurate each method is to one another without a true analysis of micro-voids which the microscopy samples in this paper were not analyzed for. Both processes have their weaknesses and strengths. The combustion process works well on fiberglass but leaves a residue on carbon substrates which then interfere with weight measurements. Combustion sampling provides a void measurement of a sample throughout its volume whereas microscopy predicts what the through-volume void content is by analyzing one side. Microscopy yields quicker results than the tedious process of combustion and provides more useful information including: void location, shape, and distribution within a sample.

5.1.3 Ultrasound and Microscopy Correlation

It is clear to see a large area of low porosity covering the top half (by the inlet) of the laminate, that begins to transform into a strip of high attenuation as the scans approached the flow front. A direct comparison of micro-voids to macro-voids was not able to be performed since no samples contained a significant reading of micro-voids along with no macro-voids, i.e. any sample with micro-voids also contained a significant amount of macro-voids. The resultant attenuation in micro-void c-scan measurements shows an increased range without any measured micro-voids followed by a wide range of attenuation for the different concentrations of measured micro-voids. This is suspected to be in part of the limitations of resolution in c-scan equipment, where the ultrasound wavelengths are too large to pick up the micro-voids in a composite laminate.

A lack of a clear correlation between c-scan attenuation and void content was noticed through all of the fiberglass panels. When graphed the other laminates showed almost no slope in linear fits to the data, or the slope was slightly negative, implying an error in the measurement method. Laminate D did show that as void content of macro-voids in the sample increased, so did the c-scan attenuation. This relationship is not as prevalent as the carbon fiber samples, but it does continue to validate the effectiveness of c-scan attenuation to determine a quick, NDT value of void content in a sample.

5.2 Void Modeling

5.2.1 Micro-void Formation and Dispersion

According to the model a large amount of micro-voids were formed during infusion, but only few remained entrapped in the resin. This implies that all of these air bubbles are diffused into molecules and dissolved in the resin. An assumption is made that the small diffused molecules of air constituents continue to travel with the flow of the resin and only become detectable once pressure drops below the threshold. In this case, this would occur once the mold was vented when infusion was cut-off.

As the pressure decreases other dissolved micro-voids traveling along the flow front will come out of solution. It is assumed that these come out as nano-voids that are unable to be measured with standard microscopy procedures. Further research will need to be done to determine whether these nano-voids have any effect on mechanical characteristics. It can be concluded that micro-void formation follows the model developed by Breard but that model only considers the formation of such voids. It does not predict what becomes of them and whether or not they will remain in the laminate or if they will escape or dissolve as seen in these trials. This model will need to be coupled with pressure threshold predictions in order to fully predict void behavior.

5.2.2 Macro-void Formation and Dispersion

The rate of macro-void formation appears to increase as the overall pressure and flow rate decrease across the laminate. Bubbles of all sizes continue to form but the amount of pressure available to shrink the bubbles to a critical size is also decreasing. It is possible that if the pressure gradient was such that it remained high enough to compress voids that over time the

laminate would reach equilibrium and all bubbles would be dissolved into solution. This would require another set of tests that could be performed in the future. As seen through these test, the predicted macro-void formation far exceeds the measured void content. This could be attributed to the continuous pressure acting on the macro-voids formed behind the flow front that is able to shrink the bubbles to critical size and allow move quickly between the tows towards the flow front and escape. Breard's model shows strong correlation of void formation when coupled with void mobility theory. Overall void formation when coupled with an optimal flow velocity as displayed in figure 2-2 could be irrelevant if enough pressure is available to minimize voids.

5.3 Mechanical Characteristics

There is a quick decrease in mechanical properties after the first 1-2% of voids. Higher levels of ILSS before failure could be due to the higher infusion flow rate. Depictions in carbon fiber laminates show an increased area of lower void content as well in laminates infused at higher rates. It is suspected that the higher flow rates should produce increased volumes of micro-voids than macro-voids per the dual-scale models illustrated in figure 2-2.

When comparing the ILSS to v_0, similar curves were evident for both macro- and micro-void percentage, but the ILSS sample in this case is compared to a sample that has both macro- and micro-voids, so there is no way to determine from these results which type of void is contributing to the loss in ILSS. Future studies must focus on imaging of actual crack imitation and propagation to clarify the effects of voids of differing size and location.

A slight decrease in SBS was noticed in laminates A-F as v_0 increased but not as drastically as represented in the laminates G and H. The lower clarity in the exponential trend could be due to the lack of samples with v_0 greater than 0% but less than 1%. Potentially if there were samples of the same material, dimensions and processing methods but with lower v_0 there

would be a more straightforward relationship as predicted and seen previously. It can be concluded that strength is not well correlated to void content above 2% and could possibly be related to void morphology.

When graphed together, an apparent upward trend in SBS is seen as distance between voids increases. This can be attributed to an increased force needed for a crack to propagate to the nearest weak area or void. There was also a slight correlation that displayed an increase in SBS as the voids were more spherical in shape but could not be completely ruled as true with the data acquired. Further accumulation of data would be required.

Each method of void measurement has determined a different void content in the end. Comparing the trends of macro-void measurement via microscopy versus SBS shows a slightly declining trend; as void content increases, SBS decreases (see figure 4-17). In contrast, when comparing percent attenuation from c-scan measurements, SBS shows a slightly increasing trend. The accuracy of void measurement and local attenuation measurement plays a significant role in the refinement of comparisons between mechanical properties and void location and percent. It is predicted that with more time and better polished microscopy samples where a micro-void measurement could be taken, a more defined trend would appear and correlate more closely with hypothesized relationships between void content and SBS.

5.4 Hypothesis Validation

The hypothesis was not able to be validated, that application of different driving pressures would result in any significant difference in measured void content or resulting mechanical properties. Thus the data failed to reject the null hypothesis. Void formation was not affected by this range of injection pressure in the fiberglass laminates and failed to show strong correlation between void content and mechanical properties. Despite the alteration in injection

pressures the flow rates results may have been more similar than intended due to irregular flow in the mold due to race-tracking.

REFERENCES

Ahn, K. J., J. C. Seferis, and J. C. Berg. "Simultaneous measurements of permeability and capillary pressure of thermosetting matrices in woven fabric reinforcements." *Polymer composites* 12.3 (1991): 146-152.

Ahlborn, H. *Characterization of binder application on carbon fibre non-crimped fabric: permeability and flow modeling*. Diss. University of Stuttgart, 2009

Cann, M. T., D. O. Adams, and C. L. Schneider. "Characterization of fiber volume fraction gradients in composite laminates." *Journal of composite materials* 42.5 (2008): 447-466.

Darcy, H. Les Fontaines Publiques De La Ville De Dijon. Paris: Dalmont, 1856.

Dungan, F. D., and A. M. Sastry. "Saturated and unsaturated polymer flows: microphenomena and modeling." *Journal of Composite Materials* 36.13 (2002): 1581-1603.

Frishfelds, V., A. Jakovics, and T. S. Lundström. "Automatic recognition and analysis of scanned non-crimp fabrics for calculation of their fluid flow permeability." *Journal of reinforced plastics and composites* 26.3 (2007): 285-296.

Frishfelds, V., T. S. Lundström, and A. Jakovics. "Bubble motion through non-crimp fabrics during composites manufacturing." *Composites Part A: Applied Science and Manufacturing* 39.2 (2008): 243-251.

Fullwood, D. T., Gerrard, D. D., George, A. R., and Halverson, D. M. "Dispersion metrics for composites – a machine learning based analysis." *Proceedings of SAMPE Tech – Conference and Exhibition*, Wichita (USA), October 21-24, (2013).

García, J. A., et al. "An efficient solver of the saturation equation in liquid composite molding processes." *International journal of material forming* 3.2 (2010): 1295-1302.

George, A., Dart, R., Brandley, M., Zsiros, J. "Quick measurement of void content in fiberglass reinforced composite materials." *Proceedings of SAMPE Tech – Conference and Exhibition*, Wichita (USA), October 21-24, (2013).

George, A. *Optimization of resin infusion processing for composite materials: simulation and characterization strategies*. Diss. University of Stuttgart, 2011.

George, A., Brandley, M., Dart, R., Peterson, C. "Characterization and optimization of optical 3D wetting measurements of through-thickness permeability." *Proceedings of 12th International Conference on Flow Processes in Composite Materials*, Twente (Netherlands), July 14-16, (2014.)

Gueroult,S., L. Bizet, & J. Breard. "Experimental determination of void formation and transport in the RTM process." *Proceedings of ICCM19*, Montreal, Canada (2013): 2218-27.

Gourichon, B., C. Binetruy, and P. Krawczak. "A new numerical procedure to predict dynamic void content in liquid composite molding." *Composites Part A: applied science and manufacturing* 37.11 (2006): 1961-1969.

Kim, S. K., and I. M. Daniel. "Observation of permeability dependence on flow rate and implications for liquid composite molding." *Journal of composite materials* 41.7 (2007): 837-849.

Lai, Y.H., B. Khomami, and J. L. Kardos. "Accurate permeability characterization of preforms used in polymer matrix composite fabrication processes." *Polymer Composites* 18.3 (1997): 368-377.

Lawrence, J. M., V. Neacsu, and S. G. Advani. "Modeling the impact of capillary pressure and air entrapment on fiber tow saturation during resin infusion in LCM." *Composites Part A: Applied Science and Manufacturing*40.8 (2009): 1053-1064.

LeBel, F., et al. "Experimental characterization by fluorescence of capillary flows in the fiber tows of engineering fabrics." *Open Journal of Inorganic Non-metallic Materials* 2012 (2012).

LeBel, F., et al. "Prediction of optimal flow front velocity to minimize void formation in dual scale fibrous reinforcements." *International journal of material forming* 7.1 (2014): 93-116.

Leclerc, J. S., and E. Ruiz. "Porosity reduction using optimized flow velocity in Resin Transfer Molding." *Composites Part A: Applied Science and Manufacturing* 39.12 (2008): 1859-1868.

Liu, L., Z. S. Guo, and B. M. Zhang. "Experimental investigation of porosity and its effects on interlaminar shear strength in composite laminates." *Int SAMPE Sym* 51 (2006): 1-7.

Lundstrom, T. S., B. R. Gebart, and C. Y. Lundemo. "Void formation in RTM."*Journal of Reinforced Plastics and Composites* 12.12 (1993): 1339-1349.

Lundström, T. S. "Measurement of void collapse during resin transfer moulding." *Composites Part A: Applied Science and Manufacturing* 28.3 (1997): 201-214.

Lundström, T. S., V. Frishfelds, and A. Jakovics. "Bubble formation and motion in non-crimp fabrics with perturbed bundle geometry." *Composites Part A: Applied Science and Manufacturing* 41.1 (2010): 83-92.

Michaud, V., et al. "Capillary phenomena in liquid composite moulding."*1CD-ROM proceedings of the Sixtennth International Conference on Composite Materials, July 8-13, 2007, Kyoto, Japan: A giant step towards environmental awareness: from green composites to aerospace*. Kyōto, 2007.

Park, C. H., et al. "Modeling and simulation of voids and saturation in liquid composite molding processes." *Composites Part A: Applied Science and Manufacturing* 42.6 (2011): 658-668.

Patel, N., and L. J. Lee. "Modeling of void formation and removal in liquid composite molding. Part II: Model development and implementation." *Polymer Composites* 17.1 (1996): 104-114.

Ravey, C., E. Ruiz, and F. Trochu. "Determination of the optimal impregnation velocity in Resin Transfer Molding by capillary rise experiments and infrared thermography." *Composites Science and Technology* 99 (2014): 96-102.

Ruiz, E., et al. "Optimization of infusion flow rate to minimize micro/macro-voids formation in resin transfer molded composites." *Composites science and technology* 66.3 (2006): 475-486.

Sisodia, S., et al. "Effects of voids on quasi-static and tension fatigue behaviour of carbon-fibre composite laminates." *Journal of Composite Materials*(2014): 0021998314541993.

Vernet, N., et al. "Experimental determination of the permeability of engineering textiles: Benchmark II." *Composites Part A: Applied Science and Manufacturing* 61 (2014): 172-184.

Verrey, J., V. Michaud, and J-AE Månson. "Dynamic capillary effects in liquid composite moulding with non-crimp fabrics." *Composites Part A: Applied Science and Manufacturing* 37.1 (2006): 92-102.

APPENDICES

APPENDIX A. VOID MEASUREMENTS

A.1 Microscopy v_0 Measurements for Laminates A-F

	left vs middle vs right comparison							
	Infusion Pressure		left (sample 4)		middle (sample 12)		right (sample 21)	
Laminate	(bar)	row	average	st deviation	average	st deviation	average	st deviation
A	0.75	1	1.37	0.74	1.07	0.55	3.23	1.67
		2	3.17	3.60	1.97	1.06	3.23	1.01
		3	1.70	0.72	4.47	1.99	2.57	2.25
		4	2.53	1.24	4.57	1.72	2.20	0.50
		5	3.83	0.40	6.97	2.00	1.33	0.61
		6	5.57	1.94	3.43	1.78	2.31	0.77
B	0.75	1	1.70	1.51	0.80	0.85	3.80	1.40
		2	2.17	1.68	4.70	1.51	2.37	1.88
		3	2.53	2.08	4.33	2.20	3.93	0.45
		4	2.67	0.95	6.03	1.42	2.00	1.18
		5	2.17	1.72	3.40	3.44	2.43	1.12
		6	1.57	0.15	4.23	2.87	0.00	0.00
C	1.00	1	2.77	1.88	2.67	0.92	2.73	0.38
		2	2.17	0.21	3.47	1.15	2.57	0.64
		3	2.13	1.34	7.97	4.86	1.33	0.51
		4	1.17	0.47	5.93	3.81	2.80	1.05
		5	2.87	0.98	0.00	0.00	1.53	0.64
		6	2.20	1.35	0.47	0.25	0.00	0.00
D	1.00	1	1.10	0.85	2.90	1.59	2.23	1.61
		2	1.80	1.54	4.30	2.34	1.43	0.98
		3	1.23	0.57	3.90	1.30	3.53	0.78
		4	3.90	2.69	2.70	1.08	3.17	0.47
		5	2.73	1.72	3.53	0.93	3.77	0.81
		6	2.23	0.75	6.63	2.59	7.90	2.72
E	1.20	1	3.53	0.35	2.17	1.57	2.47	1.01
		2	0.63	0.31	1.73	0.65	1.90	0.87
		3	1.27	0.31	2.70	2.35	3.33	2.48
		4	1.90	1.80	2.20	1.15	3.23	1.81
		5	2.13	0.83	2.90	0.62	4.77	0.90
		6	1.90	0.26	2.70	0.89	2.57	0.21
F	1.20	1	0.57	0.35	0.50	0.61	2.30	1.83
		2	1.27	1.55	2.07	1.61	3.03	1.55
		3	1.37	0.47	4.40	1.65	5.07	0.97
		4	3.80	2.45	2.50	2.09	3.93	1.11
		5	5.80	1.76	3.83	1.21	1.30	0.61
		6	4.17	0.97	3.83	1.50	2.60	0.44

A.2 Microscopy v_0 Measurements for Laminates G-H

Laminate:		Averaged by row	ILSS	sd-ILSS	Position (along flow)	v0	v0-error	Runar v0	Runar-error
ACAB	Flow Rate		tau (N/mm2)	tau (N/mm2)	mm	%	%	%	%
G	100cc/min	1	**41.24**	**0.648882238**	35	0.32%	0.39%	0.18%	0.07%
		2	**40.34**	**0.749957989**	203	0.14%	0.11%	0.06%	0.04%
		3	**37.82**	**0.598161031**	448	0.89%	0.85%	0.65%	0.17%
		4	**36.71**	**0.416784009**	471.2	2.00%	1.74%	1.77%	0.29%
		5	**36.68**	**0.760403514**	494.4	2.76%	2.75%	2.72%	0.53%
		6	**34.37**	**0.245613613**	553	5.73%	0.58%	6.20%	0.34%
		7	**34.46**	**0.689155314**	665	4.17%	0.28%	5.33%	0.32%
		Micro	v0	v0-error		Macro	v0	v0-error	
			%	%			%	%	
		1	0.05%	0.07%		1	0.27%	0.32%	
		2	0.01%	0.01%		2	0.13%	0.12%	
		3	0.07%	0.12%		3	0.81%	0.73%	
		4	0.44%	0.60%		4	1.56%	1.16%	
		5	0.53%	0.71%		5	2.22%	2.04%	
		6	2.69%	0.83%		6	3.04%	0.38%	
		7	1.55%	0.17%		7	2.62%	0.11%	

Laminate:		TOTAL	ILSS	sd-ILSS	Flow L	v0	v0-error	Runar v0	Runar-error
ACAB	Flow Rate		tau (N/mm2)	tau (N/mm2)	mm	%	%	%	%
H	400cc/min	1	**43.47**	**0.422655094**	30	0.13%	0.06%	0.00%	0.00%
		2	**44.02**	**0.47869515**	160	0.01%	0.01%	0.00%	0.00%
		3	**42.61**	**0.487382925**	290	0.00%	0.00%	0.00%	0.00%
		4	**42.43**	**0.836942321**	360	0.02%	0.02%	0.00%	0.00%
		5	**41.45**	**0.903208701**	400	1.57%	0.24%	0.37%	0.18%
		6	**38.24**	**0.321818708**	440	4.49%	0.43%	2.42%	0.23%
		7	**36.94**	**0.294276496**	548	6.30%	0.55%	12.26%	0.49%
		Micro	v0	v0-error		Macro	v0	v0-error	
			%	%			%	%	
		1	0.02%	0.01%		1	0.12%	0.05%	
		2	0.00%	0.00%		2	0.01%	0.01%	
		3	0.00%	0.00%		3	0.00%	0.00%	
		4	0.00%	0.00%		4	0.02%	0.02%	
		5	0.39%	0.11%		5	1.18%	0.20%	
		6	1.50%	0.20%		6	2.99%	0.39%	
		7	3.39%	0.39%		7	2.90%	0.57%	

A.3 Combustion v_0 Measurements for Laminates A & E

Laminate	Injection Pressure (bar)		fib+res	Mresin	Mfiber	Vresin	Vfiber	vf	Vair	v0	vf (correct)
			g	g	g	cc	cc	%	cc	%	%
A	0.75	4 5	0.49821	0.20809	0.29012	0.176947	0.111585	38.67%	0.008789	2.96%	37.53%
		4 20	0.52131	0.20271	0.3186	0.172372	0.122538	41.55%	0.01352	4.38%	39.73%
		5 5	0.47221	0.19215	0.28006	0.163393	0.107715	39.73%	0.016807	5.84%	37.41%
		5 13	0.57563	0.23815	0.33748	0.202509	0.1298	39.06%	0.026081	7.28%	36.22%
		5 20	0.39327	0.1632	0.23007	0.138776	0.088488	38.94%	0.013731	5.70%	36.72%
		6 5	0.48318	0.18984	0.29334	0.161429	0.112823	41.14%	0.020973	7.10%	38.22%
		6 13	0.59643	0.23947	0.35696	0.203631	0.137292	40.27%	0.022871	6.29%	37.74%
		6 21	0.41492	0.15791	0.25701	0.134277	0.09885	42.40%	0.012942	5.26%	40.17%
E	1.2	4 5	0.52553	0.2195	0.30603	0.18665	0.117704	38.67%	0.017633	5.48%	36.56%
		4 20	0.52085	0.21066	0.31019	0.179133	0.119304	39.98%	0.018153	5.73%	37.68%
		5 5	0.53918	0.22516	0.31402	0.191463	0.120777	38.68%	0.0156	4.76%	36.84%
		5 13	0.63691	0.2615	0.37541	0.222364	0.144388	39.37%	0.019325	5.01%	37.40%
		5 20	0.49012	0.19397	0.29615	0.16494	0.113904	40.85%	0.015366	5.22%	38.72%
		6 5	0.5339	0.21488	0.31902	0.182721	0.1227	40.17%	0.016613	5.16%	38.10%
		6 13	0.54991	0.22126	0.32865	0.188146	0.126404	40.19%	0.016386	4.95%	38.20%
		6 21	0.45933	0.1791	0.28023	0.152296	0.107781	41.44%	0.018424	6.62%	38.70%

APPENDIX B. SBS & ILSS RESULTS

B.1 SBS Laminates A-F

LAMINATE:	A								
INJ Date	12/3/2014								
INJ PRESSURE	0.75	Bar							
							Maximum Flexure load (N)	Modulus (Automatic) (MPa)	Short Beam Strength
Sample #	Width	Thickness	Load	SBS					
1--1	5.03	2.45	775.017	47.1670183		Maximum	829.49384	4668.62033	47.16702
1--2	5.29	2.49	759.413	43.2398592		Minimum	678.90918	678.51303	38.33479
1--3	5.40	2.49	764.513	42.6435185		Mean	776.8179	1842.13847	43.85517
1--6	5.31	2.55	796.825	44.1356486		Standard Dev	42.01598	1536.45715	2.0238
1--7	5.29	2.54	817.271	45.6181809		Coefficient o	5.40873	83.40617	4.61474
1--8	5.24	2.55	778.462	43.6945442					
1--9	5.25	2.60	817.673	44.9270879					
1--10	5.26	2.60	812.867	44.5781113					
1--11	5.06	2.61	795.208	45.1596929					
1--14	5.20	2.60	817.271	45.3367788					
1--15	5.23	2.60	829.494	45.7508825					
1--16	5.18	2.62	804.56	44.4619647					
1--17	5.23	2.55	803.444	45.182994					
1--18	5.31	2.53	755.695	42.1883723					
1--19	5.25	2.53	678.909	38.3347826					
1--22	5.24	2.44	729.758	42.8074162					
1--23	5.17	2.42	735.715	44.1026784					
1--24	5.19	2.41	710.629	42.61081					
Sample #	Width	Thickness	Load	SBS					
2--1	5.20	2.56	707.699	39.8718637		Maximum	903.38568	3974.1413	44.62692
2--2	5.19	2.60	657.229	36.5289573		Minimum	657.22852	83.13992	36.52893
2--3	5.13	2.64	749.938	41.5303252		Mean	799.9924	1909.67304	41.8868
2--6	5.14	2.73	800.14	42.7662804		Standard Dev	65.2664	1453.91342	1.98561
2--7	5.26	2.74	826.547	43.0122846		Coefficient o	8.15838	76.13415	4.74042
2--8	5.27	2.76	788.158	40.6401081					
2--9	5.27	2.86	873.595	43.4705119					
2--10	5.29	2.87	903.386	44.626934					
2--11	5.22	2.85	844.545	42.5763763					
2--14	5.25	2.85	834.254	41.8172431					
2--15	5.29	2.86	893.073	44.2717325					
2--16	5.25	2.88	885.055	43.9015377					
2--17	5.28	2.75	781.398	40.3614669					
2--18	5.24	2.71	769.603	40.6469008					
2--19	5.26	2.71	758.035	39.8837042					
2--22	5.32	2.61	785.279	42.4163318					
2--23	5.29	2.56	765.156	42.375576					
2--24	5.26	2.56	776.774	43.2643551					

LAMINATE:	A								
INJ Date	12/3/2014								
INJ PRESSURE	0.75	Bar							
							Maximum Flexure load (N)	Modulus (Automatic) (MPa)	Short Beam Strength
Sample #	Width	Thickness	Load	SBS					
3--1	5.21	2.62	723.183	39.7347475		Maximum	906.03986	3683.85365	46.24682
3--2	5.21	2.64	821.976	44.8207119		Minimum	703.19482	355.10066	38.94978
3--3	5.19	2.67	833.945	45.1356866		Mean	811.85822	1638.22732	42.57065
3--6	5.36	2.74	805.352	41.1274376		Standard Dev	59.96349	1358.8256	2.53532
3--7	5.35	2.76	772.709	39.2477143		Coefficient o	7.38596	82.94487	5.95556
3--8	5.37	2.78	775.288	38.9498011					
3--9	5.26	2.82	848.837	42.9191105					
3--10	5.16	2.83	866.704	44.5139288					
3--11	5.26	2.82	906.04	45.811423					
3--14	5.25	2.85	867.127	43.4650125					
3--15	5.21	2.81	902.744	46.2468153					
3--16	5.27	2.82	872.026	44.0079333					
3--17	5.24	2.72	813.694	42.8175867					
3--18	5.26	2.89	816.069	40.2628541					
3--19	5.06	2.69	739.398	40.7414741					
3--22	5.23	2.58	703.195	39.0854974					
3--23	5.26	2.56	745.99	41.5497638					
3--24	5.21	2.51	799.173	45.8343019					
Sample #	Width	Thickness	Load	SBS					
4--1	5.29	2.62	795.271	43.034766		Maximum	896.80383	4124.1893	46.97192
4--2	5.28	2.63	798.725	43.1388805		Minimum	707.96509	471.1	39.24693
4--3	5.32	2.64	822.584	43.9264354		Mean	811.63959	1817.77085	43.09675
4--6	5.24	2.70	740.354	39.2469254		Standard Dev	53.66919	1303.48601	2.03873
4--7	5.29	2.72	776.538	40.476169		Coefficient o	6.61244	71.70794	4.73059
4--8	5.28	2.74	796.814	41.3079587					
4--9	5.29	2.79	855.845	43.4907108					
4--10	5.33	2.78	896.804	45.3927815					
4--11	5.20	2.79	842.918	43.5751654					
4--14	5.29	2.77	862.63	44.1519999					
4--15	5.25	2.82	886.513	44.9094732					
4--16	5.28	2.79	870.133	44.3005152					
4--17	5.25	2.67	844.106	45.1635099					
4--18	5.30	2.66	805.511	42.8524081					
4--19	5.28	2.65	760.971	40.7896119					
4--22	5.19	2.55	707.965	40.1204239					
4--23	5.09	2.53	736.455	42.8912966					
4--24	5.19	2.49	809.364	46.971934					

LAMINATE:	A								
INJ Date	12/3/2014								
INJ PRESSURE	0.75	Bar							
							Maximum Flexure load (N)	Modulus (Automatic) (MPa)	Short Beam Strength
Sample #	Width	Thickness	Load	SBS					
5--1	5.23	2.57	784.696	43.7852557		Maximum	929.36993	4658.08788	89.77877
5--2	5.25	2.61	815.443	44.6328955		Minimum	765.50879	212.76676	40.04545
5--3	5.26	2.61	822.067	44.9099143		Mean	829.9547	2459.27434	45.92086
5--6	5.20	2.68	770.747	41.4796391		Standard Dev	45.86848	1629.95743	11.11007
5--7	5.32	2.67	771.155	40.7174009		Coefficient o	5.52662	66.27798	24.19394
5--8	5.31	2.70	765.509	40.0454593					
5--9	5.21	2.74	821.359	43.1525036					
5--10	5.18	2.73	854.645	45.3267534					
5--11	5.25	2.73	884.339	46.2762428					
5--14	5.59	2.73	895.841	44.0268631					
5--15	5.63	2.72	929.37	45.5168935					
5--16	5.65	2.70	838.678	41.23294					
5--17	5.64	2.62	822.603	41.751411					
5--18	5.57	2.62	862.216	44.3119492					
5--19	5.65	2.59	846.483	43.3841699					
5--22	5.64	2.55	852.52	44.4576554					
5--23	5.66	2.53	780.693	40.8888218					
5--24	5.41	2.49	820.815	45.6993408					
Sample #	Width	Thickness	Load	SBS					
6--1	5.23	2.52	663.461	37.7549964		Maximum	871.26233	4665.27586	46.70832
6--2	5.41	2.52	781.984	43.0191004		Minimum	663.46136	752.11707	37.75502
6--3	5.38	2.54	851.038	46.7083175		Mean	805.29823	2975.56487	43.61932
6--6	5.16	2.6	781.286	43.6765429		Standard Dev	53.89571	1499.79251	2.23749
6--7	5.41	2.59	773.787	41.41767		Coefficient o	6.69264	50.40362	5.12959
6--8	5.42	2.61	792.429	42.0128197					
6--9	5.24	2.65	833.095	44.9964893					
6--10	5.29	2.63	855.148	46.0989599					
6--11	5.28	2.66	862.47	46.0563696					
6--14	5.24	2.66	767.619	41.3041848					
6--15	5.27	2.61	827.748	45.1344631					
6--16	5.37	2.63	819.33	43.5101005					
6--17	5.75	2.56	835.949	42.5925102					
6--18	5.81	2.58	845.226	42.2900572					
6--19	5.72	2.55	871.262	44.7995681					
6--22	4.81	2.48	732.88	46.0783985					
6--23	5.3	2.48	755.237	43.0940163					
6--24	5.78	2.47	845.421	44.412938					

LAMINATE:	B								
INJ Date	12/4/2014								
INJ PRESSURE	0.75	Bar							
							Maximum Flexure load (N)	Modulus (Automatic) (MPa)	Short Beam Strength
Sample #	Width	Thickness	Load	SBS					
1--1	5.17	2.58	760.912	42.7844002		Maximum	874.02594	4690.82184	46.84504
1--2	5.33	2.57	809.732	44.3345427		Minimum	745.50165	617.04959	41.55913
1--3	5.32	2.58	806.216	44.0535933		Mean	814.11121	2330.4932	44.47736
1--6	5.28	2.63	803.401	43.3914297		Standard Dev	37.84942	1463.01428	1.41076
1--7	5.32	2.64	818.38	43.7019395		Coefficient of	4.64917	62.77702	3.17186
1--8	5.31	2.63	806.68	43.3223776					
1--9	5.28	2.69	855.39	45.1688704					
1--10	5.32	2.69	874.026	45.8059298					
1--11	5.34	2.69	867.983	45.3188568					
1--14	5.26	2.68	834.932	44.421358					
1--15	5.18	2.68	834.294	45.0729341					
1--16	5.17	2.68	858.314	46.4603121					
1--17	5.33	2.59	764.948	41.5591067					
1--18	5.34	2.58	821.152	44.701681					
1--19	5.22	2.56	834.666	46.8450296					
1--22	5.26	2.49	745.502	42.689885					
1--23	5.28	2.50	787.798	44.76125					
1--24	5.10	2.45	769.675	46.1989796					
Sample #	Width	Thickness							
2--1	4.90	2.54	745.026	44.8955086		Maximum	864.66034	4085.22403	45.75471
2--2	5.29	2.56	790.084	43.7561289		Minimum	714.46008	459.54241	39.49912
2--3	5.31	2.58	723.557	39.6113629		Mean	794.91107	2432.6581	42.80006
2--6	5.27	2.63	837.494	45.3186124		Standard Dev	50.42657	1389.15601	2.05087
2--7	5.26	2.64	743.853	40.1752614		Coefficient of	6.34367	57.10445	4.79175
2--8	5.43	2.67	766.182	39.635297					
2--9	5.24	2.73	852.854	44.7138453					
2--10	5.23	2.71	864.66	45.7546937					
2--11	5.33	2.74	859.741	44.1520761					
2--14	5.24	2.74	854.988	44.6621302					
2--15	5.34	2.74	857.3	43.9442713					
2--16	5.32	2.70	810.364	42.3122389					
2--17	5.42	2.65	800.835	41.8176043					
2--18	5.32	2.63	790.563	42.3770155					
2--19	5.25	2.59	788.582	43.4959735					
2--22	5.32	2.55	714.46	39.4991154					
2--23	5.33	2.54	765.919	42.4309916					
2--24	5.34	2.49	741.836	41.843554					

LAMINATE:	B								
INJ Date	12/4/2014								
INJ PRESSURE	0.75	Bar							
							Maximum Flexure load (N)	Modulus (Automatic) (MPa)	Short Beam Strength
Sample #	Width	Thickness	Load	SBS					
3--1	5.27	2.59	795.146	43.6915813		Maximum	857.73114	4382.47237	46.74468
3--2	5.23	2.59	707.129	39.1524063		Minimum	707.12854	616.38495	39.11076
3--3	5.31	2.58	794.343	43.4865655		Mean	789.40946	2471.37183	42.66711
3--6	5.22	2.65	832.248	45.1229668		Standard Dev	40.07009	1405.31674	2.17276
3--7	5.35	2.65	787.986	41.6850291		Coefficient of	5.07596	56.86383	5.09236
3--8	5.40	2.64	806.535	42.4313447					
3--9	5.27	2.69	856.214	45.2981737					
3--10	5.36	2.71	857.731	44.2872067					
3--11	5.33	2.71	753.237	39.1107738					
3--14	5.24	2.70	741.589	39.312394					
3--15	5.35	2.70	838.529	43.5373313					
3--16	0.00	0.00							
3--17	5.32	2.61	763.949	41.2642058					
3--18	5.40	2.59	777.375	41.6867761					
3--19	5.31	2.59	783.484	42.7264795					
3--22	5.36	2.53	766.369	42.3851653					
3--23	5.34	2.51	775.928	43.4177895					
3--24	5.04	2.49	782.169	46.7446572					
Sample #	Width	Thickness							
4--1	5.19	2.56	693.396	39.1413024		Maximum	867.34473	3994.6884	47.65875
4--2	5.30	2.58	834.03	45.7453927		Minimum	693.39648	649.95758	37.95114
4--3	5.27	2.59	867.345	47.6587627		Mean	790.83482	1722.43094	42.9062
4--6	5.14	2.63	743.426	41.2458389		Standard Dev	52.67484	1320.31874	2.5886
4--7	5.35	2.63	791.651	42.197381		Coefficient of	6.66066	76.65438	6.03317
4--8	5.35	2.64	864.461	45.9038339					
4--9	5.34	2.67	843.35	44.3625594					
4--10	5.36	2.67	789.513	41.3756184					
4--11	5.29	2.67	800.284	42.4950617					
4--14	5.32	2.68	761.611	40.0634223					
4--15	5.32	2.67	830.562	43.8541227					
4--16	5.33	2.67	851.715	44.8866391					
4--17	5.32	2.59	720.115	39.1969003					
4--18	5.32	2.58	801.25	43.782239					
4--19	5.33	2.56	815.801	44.8413132					
4--22	5.21	2.52	735.572	42.0192396					
4--23	5.30	2.49	731.405	41.5665492					
4--24	5.10	2.47	759.538	45.2213622					

LAMINATE:	B								
INJ Date	12/4/2014								
INJ PRESSURE	0.75	Bar							
							Maximum Flexure load	Modulus (Automatic)	Short Beam Strength
Sample #	Width	Thickness	Load	SBS			(N)	(MPa)	
5--1	5.37	2.58	888.589	48.1025616		Maximum	888.58887	4179.37426	48.10255
5--2	5.25	2.58	847.822	46.9447398		Minimum	695.55328	440.1553	39.45685
5--3	5.28	2.60	820.116	44.8052885		Mean	803.95065	2010.25609	43.84806
5--6	5.34	2.61	790.995	42.5650588		Standard Dev	52.5043	1486.1183	2.46439
5--7	5.37	2.65	846.746	44.626647		Coefficient of	6.53079	73.92681	5.6203
5--8	5.34	2.64	859.156	45.7075672					
5--9	5.34	2.64	782.129	41.6096889					
5--10	5.35	2.65	770.994	40.78614					
5--11	5.31	2.65	819.096	43.6571794					
5--14	5.35	2.64	855.273	45.415941					
5--15	5.31	2.64	832.205	44.5238936					
5--16	5.28	2.63	802.677	43.3523267					
5--17	5.30	2.58	719.377	39.4568341					
5--18	5.34	2.56	807.288	44.2902914					
5--19	5.33	2.55	819.4	45.2157598					
5--22	5.32	2.49	714.13	40.4322176					
5--23	5.15	2.47	695.553	41.0097677					
5--24	5.24	2.43	799.695	47.1029474					
Sample #	Width	Thickness							
6--1	5.38	2.59	847.61633	45.6224432		Maximum	850.95062	4228.24557	46.58254
6--2	5.23	2.59	801.45654	44.3751452		Minimum	588.05432	726.48854	32.90508
6--3	5.33	2.59	752.32605	40.8733647		Mean	752.79107	2072.73378	41.37266
6--6	5.27	2.61	777.59149	42.3995883		Standard Dev	87.94259	1406.15257	4.36456
6--7	5.34	2.6	850.95062	45.967514		Coefficient of	11.6822	67.84048	10.54937
6--8	5.33	2.59	806.80249	43.8330328					
6--9	5.29	2.61	789.33972	42.8774591					
6--10	5.31	2.61	844.6593	45.7096402					
6--11	5.29	2.61	810.15369	44.0080878					
6--14	5.13	2.6	828.42389	46.5825399					
6--15	5.29	2.61	791.51093	42.9954007					
6--16	5.29	2.61	766.58032	41.6411533					
6--17	5.37	2.56	659.47577	35.9787322					
6--18	5.29	2.55	732.58319	40.7307456					
6--19	5.3	2.53	588.29901	32.905083					
6--22	5.28	2.47	588.05432	33.8179932					
6--23	5.45	2.44	607.76935	34.2778623					
6--24	5.38	2.41	706.6463	40.87559					

LAMINATE:	C								
INJ Date	9/16/2014								
INJ PRESSURE	1	Bar							
							Maximum Flexure load (N)	Modulus (Automatic) (MPa)	Short Beam Strength
Sample #	Width	Thickness	Load (N)	SBS					
1--1	5.19	2.59	525.20	29.3031781		Maximum	139.64374	9114.43077	76.91624
1--2	5.15	2.63	795.26	44.0358448		Mean	98.71662	6694.02619	52.83281
1--3	5.12	2.63	802.28	44.6847523		Standard Deviation	21.07767	2524.83786	11.0473
1--6	5.02	2.71	751.13	41.4097117		Minimum	50.3142	1074.73105	28.9689
1--7	5.16	2.71	777.64	41.7081438					
1--8	5.12	2.73	788.92	42.3314625					
1--9	5.21	2.78	793.31	41.0793783					
1--10	5.26	2.79	854.69	43.6799338					
1--11	5.09	2.79	844.47	44.5988339					
1--14	5.07	2.78	908.69	48.3531459					
1--15	5.20	2.79	881.30	45.5593466					
1--16	5.16	2.80	875.94	45.4702554					
1--17	5.25	2.77	846.15	43.6383187					
1--18	5.10	2.75	786.51	42.0591444					
1--19	5.14	2.77	812.07	42.7770442					
1--22	5.15	2.70	867.61	46.7964401					
1--23	5.22	2.69	825.76	44.1052429					
1--24	5.24	2.65	493.41	26.6498992					
Sample #	Width	Thickness							
2--1	LOST	LOST				Maximum	154.22508	8562.83282	74.70519
2--2	5.16	2.71	946.44	50.7617137		Mean	114.10894	6519.78478	57.47907
2--3	5.08	2.74	947.05	51.0291719		Standard Deviation	26.78998	1817.71194	12.50369
2--6	5.11	2.82	894.56	46.5587396		Minimum	36.63587	1962.54286	19.63739
2--7	5.14	2.81	882.12	45.8055409					
2--8	5.23	2.84	900.36	45.4626781					
2--9	5.14	2.95	830.45	41.0763371					
2--10	5.18	2.93	881.83	43.5758924					
2--11	5.09	2.94	833.81	41.7889219					
2--14	5.1	2.94	838.05	41.9194678					
2--15	5.09	2.92	830.921	41.9295658					
2--16	5.11	2.92	852.09	42.8293971					
2--17	5.21	2.86	907.73	45.6890662					
2--18	5.17	2.86	899.86	45.6434716					
2--19	5.29	2.83	838.24	41.993878					
2--22	5.15	2.78	939.38	49.209576					
2--23	5.17	2.76	945.86	49.7150681					
2--24	5.09	2.72	335.72	18.1865032					

LAMINATE:	C								
INJ Date	9/16/2014								
INJ PRESSURE	1	Bar							
							Maximum Flexure load (N)	Modulus (Automatic) (MPa)	Short Beam Strength
Sample #	Width	Thickness	Load (N)	SBS					
3--1	5.22	2.7	759.16	40.3978821		Maximum	133.37642	8724.33969	67.51982
3--2	5.14	2.72	933.31	50.0671993		Mean	101.25027	5988.57654	52.53466
3--3	5.1	2.73	907.56	48.8882245		Standard Deviation	20.27503	2302.40581	9.35411
3--6	5.18	2.8	884.32	45.7282819		Minimum	41.66687	1656.88176	23.25431
3--7	5.12	2.8	869.08	45.4665527					
3--8	5.15	2.83	881.02	45.3370098					
3--9	5.15	2.87	824.04	41.8137749					
3--10	5.06	2.88	847.95	43.640275					
3--11	5.08	2.87	841.10	43.2675451					
3--14	5.08	2.86	832.04	42.9511384					
3--15	5.1	2.86	867.40	44.6009358					
3--16	4.98	2.86	884.33	46.5671076					
3--17	5.19	2.77	861.83	44.9607688					
3--18	5.08	2.78	866.42	46.0131245					
3--19	5.05	2.74	881.44	47.7763605					
3--22	5.07	2.7	914.80	50.1204799					
3--23	5.08	2.64	917.11	51.2881398					
3--24	5.03	2.62	408.61	23.254291					
Sample #	Width	Thickness							
4--1	5.11	2.68	717.26	39.281187		Maximum	124.32302	8423.93111	67.08049
4--2	5.09	2.71	927.20	50.413643		Mean	104.7556	5993.91383	54.85056
4--3	5.15	2.72	873.54	46.7702741		Standard Deviation	20.98022	2559.34579	10.5698
4--6	5.04	2.78	901.02	48.2302908		Minimum	45.00225	1095.94139	24.91145
4--7	5.15	2.78	911.99	47.7746909					
4--8	4.96	2.79	876.00	47.4766411					
4--9	5.17	2.83	802.06	41.1142361					
4--10	5.16	2.84	841.44	43.064148					
4--11	5.19	2.83	813.06	41.5173921					
4--14	5.04	2.84	818.27	42.8753249					
4--15	4.12	2.83	838.42	53.9312241					
4--16	5.04	2.83	845.85	44.4774314					
4--17	5.12	2.73	871.81	46.7786852					
4--18	5.11	2.73	873.29	46.9500118					
4--19	5.03	2.71	891.40	49.0452671					
4--22	5.01	2.65	909.05	51.3528415					
4--23	5.14	2.63	889.14	49.3298849					
4--24	5.13	2.59	441.32	24.911434					

LAMINATE:	C								
INJ Date	9/16/2014								
INJ PRESSURE	1	Bar							
							Maximum Flexure load (N)	Modulus (Automatic) (MPa)	Short Beam Strength
Sample #	Width	Thickness	Load (N)	SBS					
5--1	5.14	2.65	769.14	42.3504148		Maximum	1141.35681	4456.59032	61.80187
5--2	5.12	2.68	886.587	48.4593816		Minimum	498.32919	316.08756	28.23822
5--3	5.13	2.7	1141.357	61.8018735		Mean	930.82049	2860.37686	49.89967
5--6	5.04	2.76	981.519	52.9200634		Standard Deviation	159.23443	1398.4898	8.05771
5--7	5.06	2.74	1071.658	57.9717478		Coefficient of Variation	17.10689	48.8918	16.14782
5--8	5.21	2.77	1122.546	58.3375139					
5--9	5.07	2.82	800.968	42.0164505					
5--10	5.11	2.83	904.774	46.9238934					
5--11	5.05	2.81	976.43	51.6065325					
5--14	5.09	2.8	1117.833	58.8250596					
5--15	5.08	2.83	814.903	42.5125379					
5--16	5.1	2.81	1056.627	55.297624					
5--17	5.17	2.73	1069.289	56.8202542					
5--18	5.08	2.72	896.548	48.6633714					
5--19	5.13	2.7	877.406	47.50953					
5--22	5.16	2.66	907.295	49.5767945					
5--23	5.14	2.61	861.56	48.1662865					
5--24	5.15	2.57	498.329	28.2382041					
Sample #	Width	Thickness							
6--1	5.06	2.63	587.717	33.1225109		Maximum	1052.88733	4351.42022	55.85254
6--2	5.04	2.65	919.901	51.656615		Minimum	320.97919	509.90428	18.6203
6--3	5.13	2.72	904.792	48.6321809		Mean	795.52024	1211.81703	43.26254
6--6	5.11	2.71	883.855	47.8687509		Standard Deviation	157.8633	1110.24539	8.26533
6--7	5.16	2.74	1052.887	55.8525187		Coefficient of Variation	19.84403	91.61824	19.10505
6--8	5.09	2.72	994.836	53.8922195					
6--9	5.15	2.74	856.208	45.5074764					
6--10	5.2	2.77	754.231	39.2719557					
6--11	5.05	2.82	838.397	44.1540447					
6--14	5.06	2.76	843.584	45.3033167					
6--15	5.18	2.76	771.223	40.4578122					
6--16	5.05	2.76	816.456	43.9332759					
6--17	5.17	2.69	714.756	38.5457278					
6--18	5.07	2.68	750.52	41.426742					
6--19	5.11	2.64	689.13	38.3122443					
6--22	5.19	2.58	743.262	41.6309316					
6--23	5.05	2.56	871.943	50.5845645					
6--24	5.09	2.54	800.206	46.4206875					

LAMINATE:	D									
INJ Date	11/16/2014									
INJ PRESSURE	1	Bar								
								Maximum Flexure load (N)	Modulus (Automatic) (MPa)	Short Beam Strength
Sample #	Width	Thickness	Load kgf)	SBS						
1--1	5.17	2.58	762.83905	42.8927539			Maximum	867.9469	4013.92458	46.12127
1--2	5.47	2.58	799.50372	42.4888249			Minimum	663.15674	466.67953	37.29203
1--3	5.12	2.59	796.16467	45.0292217			Mean	783.09241	2476.28621	42.81565
1--6	5.06	2.69	787.10309	43.3700661			Standard Dev	47.92302	1332.90729	2.21335
1--7	5.15	2.68	795.79095	43.243241			Coefficient of	6.11971	53.82687	5.16949
1--8	5.16	2.67	783.5014	42.6520665						
1--9	5.06	2.72	785.97571	42.8302853						
1--10	5.11	2.73	852.38647	45.8262441						
1--11	5.17	2.73	867.9469	46.121267						
1--14	5.18	2.72	724.6908	38.5758361						
1--15	5.19	2.71	782.82886	41.7437483						
1--16	5.14	2.72	768.76776	41.2405456						
1--17	5.43	2.68	841.65845	43.3773012						
1--18	5.11	2.73	823.88007	44.2936749						
1--19	5.02	2.66	759.6272	42.6654585						
1--22	5.11	2.61	663.15674	37.2920316						
1--23	5.07	2.58	741.01099	42.4872133						
1--24	4.99	2.56	758.83063	44.5518359						
Sample #	Width	Thickness					Maximum	920.96368	4053.78301	46.88663
2--1	5.23	2.65	850.47949	46.0232777			Minimum	761.84454	128.541	39.77885
2--2	5.15	2.69	848.70367	45.9470713			Mean	844.25428	1768.25936	43.6552
2--3	5.11	2.7	829.94653	45.1155974			Standard Dev	35.22779	1315.2566	2.095
2--6	5.02	2.79	761.84454	40.7961991			Coefficient of	4.17265	74.38143	4.79898
2--7	5.13	2.8	856.85675	44.7398052						
2--8	5.2	2.82	843.27423	43.1298195						
2--9	5.2	2.92	859.47931	42.4532062						
2--10	5.2	2.92	854.33069	42.1988947						
2--11	5.14	2.92	856.84137	42.8169492						
2--14	5.12	2.92	920.96368	46.2009552						
2--15	5.14	2.91	896.33685	44.9444848						
2--16	5.14	2.92	850.0946	42.4798085						
2--17	5.15	2.86	839.95966	42.7707071						
2--18	5.16	2.84	824.36017	42.1900677						
2--19	5.24	2.79	802.80035	41.1844553						
2--22	5.15	2.72	794.93549	42.561509						
2--23	5.12	2.72	847.55682	45.6447908						
2--24	5.12	2.68	857.81281	46.8866318						

LAMINATE:	D									
INJ Date	11/16/2014									
INJ PRESSURE	1	Bar								
								Maximum Flexure load (N)	Modulus (Automatic) (MPa)	Short Beam Strength
Sample #	Width	Thickness	Load kgf)	SBS						
3--1	4.88	2.62	777.00891	45.5791424			Maximum	874.49261	3974.70642	55.63233
3--2	5.12	2.64	806.948	44.7747248			Minimum	762.20837	372.06094	40.63319
3--3	5.11	2.68	832.20862	45.576165			Mean	817.11365	2154.21564	44.50139
3--6	5.17	2.76	773.07074	40.6331858			Standard Dev	37.18213	1225.277	3.29001
3--7	5.14	2.76	811.5011	42.9020629			Coefficient o	4.55042	56.8781	7.39304
3--8	5.07	2.78	814.64117	43.3485787						
3--9	5.09	2.84	862.34265	44.74093						
3--10	0	EATEN								
3--11	5.19	2.86	861.01263	43.5048218						
3--14	5.19	2.85	874.49261	44.34097						
3--15	0	EATEN								
3--16	5.09	2.85	852.79883	44.0905196						
3--17	5.14	2.76	855.8291	45.245575						
3--18	5.12	2.76	833.42401	44.2331867						
3--19	5.14	2.72	789.77161	42.3672971						
3--22	5.2	2.64	762.20837	41.6416286						
3--23	5.12	2.6	768.02222	43.2704826						
3--24	5.14	2.58	798.53778	45.162077						
Sample #	Width	Thickness								
4--1	4.88	2.63	754.40326	44.084838			Maximum	868.18365	6745.88491	82.37952
4--2	5.11	2.63	838.37531	46.7867733			Minimum	754.40326	448.49567	41.6789
4--3	5.13	2.65	803.76874	44.343415			Mean	808.1147	2940.99151	45.92352
4--6	5.06	2.73	768.83252	41.7426335			Standard Dev	31.04792	1697.47879	9.20077
4--7	5.11	2.73	821.62042	44.1721909			Coefficient o	3.84202	57.71791	20.03499
4--8	5.1	2.74	786.20892	42.1967003						
4--9	5.02	2.8	818.39783	43.6680686						
4--10	5.15	2.82	868.18365	44.8349334						
4--11	5.01	2.8	805.14551	43.0467018						
4--14	5.13	2.81	863.81482	44.9426037						
4--15	5.18	2.86	823.28619	41.678905						
4--16	5.07	2.8	792.19073	41.8528492						
4--17	5.15	2.72	823.65216	44.0990234						
4--18	5.14	2.74	828.42493	44.1164686						
4--19	5.15	2.7	808.91803	43.6309617						
4--22	5.11	2.62	773.34491	43.3223796						
4--23	5.14	2.59	782.59735	44.0896604						
4--24	5.02	2.56	784.89929	45.8069649						

LAMINATE:	D									
INJ Date	11/16/2014									
INJ PRESSURE	1	Bar								
								Maximum Flexure load (N)	Modulus (Automatic) (MPa)	Short Beam Strength
Sample #	Width	Thickness	Load kgf)	SBS						
5--1	5.12	2.58	826.45239	46.9233961			Maximum	865.22546	4102.0973	46.9234
5--2	5.06	2.62	790.56427	44.7246178			Minimum	754.62878	266.3702	41.45022
5--3	5.09	2.63	799.99341	44.8202363			Mean	797.88257	2040.14406	43.59327
5--6	5	2.7	771.32013	42.8511183			Standard Dev	26.83103	1192.20254	1.48432
5--7	5.17	2.69	768.61426	41.4502236			Coefficient o	3.36278	58.43717	3.40494
5--8	5.12	2.7	765.74933	41.54456						
5--9	5.09	2.74	808.22815	43.4637197						
5--10	5.11	2.77	791.7395	41.9510569						
5--11	5.03	2.78	813.82886	43.6497308						
5--14	5.17	2.76	865.22546	45.476908						
5--15	5.21	2.75	826.75519	43.2780592						
5--16	5.1	2.78	796.16138	42.1160273						
5--17	5.16	2.69	810.71863	43.80558						
5--18	5.19	2.69	816.8089	43.8795421						
5--19	5.14	2.66	780.5705	42.8182232						
5--22	5.14	2.6	754.62878	42.3504628						
5--23	5.11	2.59	780.95587	44.2554838						
5--24	5.13	2.56	793.57123	45.3199944						
Sample #	Width	Thickness								
6--1	5.13	2.56	837.82153	47.8470812			Maximum	837.82153	4496.01921	47.84708
6--2	5.16	2.57	807.62207	45.6758478			Minimum	708.05121	783.86498	40.92185
6--3	5.18	2.59	825.25378	46.1338035			Mean	779.585	2742.70696	43.51456
6--6	5.04	2.64	745.1792	42.0036977			Standard Dev	33.73515	1354.5049	1.69356
6--7	5.15	2.66	800.87799	43.8468861			Coefficient o	4.32732	49.3857	3.89193
6--8	5.13	2.65	789.51678	43.5571433						
6--9	5.14	2.7	779.79608	42.1420277						
6--10	5.17	2.7	789.85486	42.4379357						
6--11	5.11	2.68	806.65051	44.1764672						
6--14	5.19	2.69	787.84198	42.323419						
6--15	5.11	2.73	761.16272	40.9218468						
6--16	5.15	2.69	777.47076	42.0906681						
6--17	5.15	2.63	790.77948	43.7878556						
6--18	5.19	2.62	798.8114	44.0592265						
6--19	5.04	2.61	741.74988	42.2909756						
6--22	5.06	2.53	731.18506	42.8368507						
6--23	5.1	2.53	752.90472	43.7633527						
6--24	4.84	2.53	708.05121	43.3670669						

LAMINATE:	E								
INJ Date	11/29/2014								
INJ PRESSURE	1.2	Bar							
							Maximum Flexure load (N)	Modulus (Automatic) (MPa)	Short Beam Strength
Sample #	Width	Thickness	Load	SBS					
1--1	4.75	2.50	700.75098	44.2579566		Maximum	798.15991	4255.60624	45.15501
1--2	5.00	2.53	744.81079	44.1587425		Minimum	692.86816	372.14703	34.20487
1--3	4.99	2.53	731.76849	43.4724285		Mean	761.74512	2956.97014	43.2738
1--6	5.01	2.57	740.30701	43.1223357		Standard Deviation	34.23605	1448.53343	2.46192
1--7	5.05	2.57	748.75629	43.2690386		Coefficient of Variation	4.49442	48.98708	5.68918
1--8	5.14	2.61	788.23621	44.0670541					
1--9	5.05	2.66	781.09613	43.6106676					
1--10	5.01	2.67	777.20074	43.5758113					
1--11	4.99	2.66	793.80219	44.8529874					
1--14	4.98	2.70	783.39728	43.6968585					
1--15	4.96	2.69	787.30841	44.256004					
1--16	4.91	2.70	798.15991	45.1550074					
1--17	5.06	2.68	791.80914	43.7921697					
1--18	5.04	2.67	777.73248	43.3460674					
1--19	4.98	2.65	792.00623	45.0105837					
1--22	5.08	2.61	773.89807	43.7764769					
1--23	5.93	2.59	700.45648	34.2048715					
1--24	5.05	2.55	768.79224	44.7753197					
Sample #	Width	Thickness							
2--1	4.97	2.62	692.86816	39.9074692		Maximum	923.11853	3237.69525	46.72409
2--2	5.06	2.66	781.77686	43.5624123		Minimum	729.56824	338.40635	39.2241
2--3	5.06	2.69	767.28906	42.2782958		Mean	813.35618	1628.63546	42.98916
2--6	4.82	2.78	743.42615	41.6109147		Standard Deviation	59.60823	1048.45486	1.99825
2--7	5.11	2.79	792.80353	41.7063069		Coefficient of Variation	7.32867	64.37628	4.64826
2--8	5.08	2.80	762.48773	40.2042884					
2--9	5.05	2.93	860.25641	43.6043867					
2--10	5.03	2.94	864.62311	43.850322					
2--11	5.11	2.94	890.55438	44.458364					
2--14	4.94	2.93	885.08075	45.8616409					
2--15	5.04	2.94	923.11853	46.7240915					
2--16	5.09	2.97	842.3161	41.7890149					
2--17	5.08	2.85	834.95221	43.2528082					
2--18	5.01	2.82	796.52332	42.2836943					
2--19	5.00	2.79	729.56824	39.2240989					
2--22	5.10	2.72	848.2937	45.86363					
2--23	4.75	2.71	736.3327	42.9014974					
2--24	5.14	2.69	767.65234	41.6399733					

LAMINATE:	E								
INJ Date	11/29/2014								
INJ PRESSURE	1.2	Bar							
							Maximum Flexure load (N)	Modulus (Automatic) (MPa)	Short Beam Strength
Sample #	Width	Thickness	Load	SBS					
3--1	5.05	2.63	784.63043	44.3077079		Maximum	855.50586	4119.18102	44.9722
3--2	5.08	2.64	765.08325	42.7860622		Minimum	716.64813	379.84647	38.48643
3--3	5.09	2.67	741.50732	40.9211342		Mean	789.77679	2134.33056	42.65634
3--6	5.13	2.75	828.53821	44.0477517		Standard Deviation	45.78248	1212.12429	1.87808
3--7	5.12	2.76	838.14801	44.4839085		Coefficient of Variation	5.79689	56.79178	4.40282
3--8	5.05	2.79	844.84778	44.9722016					
3--9	5.05	2.86	844.47778	43.85227					
3--10	5.10	2.86	832.63849	42.8135793					
3--11	5.07	2.86	839.66901	43.4305566					
3--14	4.95	2.86	741.79993	39.2985765					
3--15	5.03	2.85	796.617	41.6771476					
3--16	5.06	2.83	855.50586	44.8071478					
3--17	5.06	2.76	716.64813	38.4864308					
3--18	5.04	2.73	760.97504	41.4799756					
3--19	4.85	2.72	749.58276	42.6157573					
3--22	5.10	2.66	762.22888	42.140031					
3--23	5.10	2.62	733.70502	41.1823653					
3--24	5.09	2.58	779.37927	44.5115405					
Sample #	Width	Thickness							
4--1	5.12	2.62	774.83356	43.3209961		Maximum	813.58368	4077.78939	44.09611
4--2	5.07	2.63	766.72705	43.1259168		Minimum	707.17688	527.93338	39.91261
4--3	5.07	2.67	795.89941	44.0961045		Mean	768.05118	2408.52256	42.24535
4--6	5.06	2.72	759.27075	41.3750481		Standard Deviation	28.78592	1297.41783	1.31624
4--7	5.07	2.74	801.02112	43.2460761		Coefficient of Variation	3.74792	53.86779	3.11572
4--8	5.07	2.75	791.77887	42.5916552					
4--9	4.84	2.82	794.20654	43.6415586					
4--10	5.07	2.83	813.58368	42.5274259					
4--11	4.93	2.81	787.75433	42.6480151					
4--14	5.00	2.81	744.71289	39.7533571					
4--15	5.05	2.80	789.36371	41.8686551					
4--16	4.98	2.80	757.39832	40.7378614					
4--17	5.06	2.71	743.97479	40.6911229					
4--18	4.94	2.69	707.17688	39.9126063					
4--19	5.01	2.68	735.60297	41.0896288					
4--22	5.12	2.61	783.6261	43.9804519					
4--23	5.07	2.58	736.86511	42.2495017					
4--24	5.02	2.54	741.12518	43.5928636					

LAMINATE:	E								
INJ Date	11/29/2014								
INJ PRESSURE	1.2	Bar							
							Maximum Flexure load (N)	Modulus (Automatic) (MPa)	Short Beam Strength
Sample #	Width	Thickness	Load	SBS					
5--1	4.98	2.60	718.71332	41.630753		Maximum	873.91846	4561.83943	57.89729
5--2	5.05	2.60	764.57025	43.6730912		Minimum	686.36139	403.8268	37.86612
5--3	5.05	2.63	777.37518	43.8980074		Mean	780.19367	1867.75017	43.98289
5--6	5.10	2.70	738.31671	40.2133284		Standard Deviation	55.15979	1389.89292	4.35546
5--7	5.04	2.72	725.17004	39.673606		Coefficient of Variation	7.07001	74.41535	9.90263
5--8	5.09	2.72	762.31995	41.2963685					
5--9	5.07	2.78	873.91846	46.5028341					
5--10	5.09	2.79	848.58734	44.8162822					
5--11	4.95	2.76	851.62671	46.7515761					
5--14	5.05	2.77	809.30273	43.3911461					
5--15	5.05	2.75	866.02771	46.7701734					
5--16	5.05	2.75	742.98242	40.1250632					
5--17	5.08	2.66	810.27429	44.9725976					
5--18	5.08	2.65	762.8313	42.4991439					
5--19	5.13	2.65	686.36139	37.8661255					
5--22	5.06	2.57	797.85046	46.0149679					
5--23	5.00	2.54	790.32684	46.6728449					
5--24	4.99	2.52	716.93091	42.7599789					
Sample #	Width	Thickness							
6--1	5.05	2.56	722.18536	41.8965826		Maximum	848.75708	4897.64177	47.07639
6--2	5	2.56	725.60168	42.5157234		Minimum	690.98761	490.50444	39.26066
6--3	5.07	2.58	768.14655	44.04308		Mean	769.70088	2855.0407	43.75249
6--6	5	2.64	690.98761	39.2606597		Standard Deviation	43.51994	1563.23061	2.19579
6--7	5.05	2.65	720.00586	40.3515333		Coefficient of Variation	5.65414	54.75336	5.01866
6--8	5.1	2.66	745.91254	41.2379777					
6--9	4.99	2.7	788.56323	43.8968621					
6--10	5.07	2.69	808.20239	44.4448203					
6--11	5.1	2.7	848.75708	46.2285991					
6--14	5.14	2.69	795.5799	43.1548555					
6--15	5.07	2.69	826.15381	45.4320082					
6--16	5.09	2.68	805.85461	44.3062896					
6--17	5.03	2.6	775.81976	44.491881					
6--18	5.03	2.57	803.25415	46.6029204					
6--19	4.94	2.56	793.79578	47.0763881					
6--22	5.18	2.52	749.28601	43.0505384					
6--23	5.05	2.47	774.48322	46.5677168					
6--24	5.05	2.46	712.02631	42.9863747					

LAMINATE:	F								
INJ Date	12/2/2014								
INJ PRESSURE	1.2	Bar							
							Maximum Flexure load	Modulus (Automatic)	Short Beam Strength
Sample #	Width	Thickness	Load	SBS			(N)	(MPa)	
1--1	5.09	2.56	733.7326	42.2319691		Maximum	838.76086	4200.42177	47.48712
1--2	5.11	2.55	668.21368	38.4605549		Minimum	668.21368	685.12404	38.46055
1--3	5.10	2.56	710.25409	40.8004418		Mean	759.56431	1802.00048	43.2733
1--6	4.90	2.61	809.75043	47.4871235		Standard Deviation	47.44202	1199.7569	2.28708
1--7	5.14	2.63	804.98901	44.6614015		Coefficient of Variation	6.24595	66.57917	5.28519
1--8	5.10	2.64	784.31799	43.6897276					
1--9	5.08	2.67	780.76807	43.1726129					
1--10	5.07	2.67	800.48016	44.3498969					
1--11	5.05	2.69	796.0072	43.9475432					
1--14	4.94	2.68	744.01849	42.1486092					
1--15	5.07	2.66	838.76086	46.6455076					
1--16	5.03	2.67	824.76166	46.0585733					
1--17	5.11	2.58	739.08752	42.04521					
1--18	5.07	2.57	741.005	42.6521884					
1--19	5.14	2.55	692.20856	39.6090959					
1--22	5.07	2.48	744.98962	44.4377279					
1--23	5.15	2.48	735.56812	43.1941818					
1--24	5.11	2.45	723.24451	43.3270804					
Sample #	Width	Thickness							
2--1	5.05	2.71	764.26746	41.883789		Maximum	882.22528	4063.57916	44.76209
2--2	5.07	2.70	725.26129	39.73599		Minimum	707.18109	171.39492	39.73599
2--3	5.07	2.74	753.47821	40.679297		Mean	795.43793	1946.12422	42.1994
2--6	5.04	2.84	802.50977	42.0496819		Standard Deviation	55.93947	1411.89794	1.4026
2--7	5.05	2.84	797.88373	41.7245013		Coefficient of Variation	7.03254	72.54922	3.32374
2--8	5.09	2.85	826.69769	42.7410656					
2--9	5.08	2.93	832.02881	41.9245389					
2--10	5.08	2.93	869.35779	43.8054838					
2--11	5.02	2.93	844.36487	43.0546519					
2--14	5.10	2.92	882.22528	44.4311684					
2--15	5.04	2.90	872.32367	44.7620931					
2--16	5.08	2.90	822.8775	41.8923517					
2--17	5.12	2.77	816.04401	43.1544032					
2--18	5.05	2.75	807.38599	43.6032038					
2--19	5.02	2.72	743.75653	40.8525748					
2--22	5.08	2.61	707.18109	40.0025506					
2--23	5.03	2.57	715.20898	41.4947463					
2--24	5.09	2.55	735.03003	42.4725546					

LAMINATE:	F								
INJ Date	12/2/2014								
INJ PRESSURE	1.2	Bar							
							Maximum Flexure load (N)	Modulus (Automatic) (MPa)	Short Beam Strength
Sample #	Width	Thickness	Load	SBS					
3--1	5.07	2.67	838.01483	46.4294722		Maximum	842.29272	4640.42938	46.42947
3--2	5.11	2.70	808.02899	43.9241678		Minimum	710.37085	118.84687	39.49079
3--3	5.05	2.74	761.32343	41.2656336		Mean	792.79476	1826.70731	42.41302
3--6	5.01	2.79	802.01587	43.0330667		Standard Deviation	30.69274	1406.04398	2.06816
3--7	5.14	2.81	799.75018	41.5284929		Coefficient of Variation	3.87146	76.9715	4.87624
3--8	5.19	2.83	778.24451	39.7396041					
3--9	5.11	2.87	815.63464	41.7113387					
3--10	5.10	2.89	813.49805	41.3951786					
3--11	5.09	2.88	802.81067	41.0737286					
3--14	5.11	2.86	804.23474	41.2721563					
3--15	5.05	2.87	802.62219	41.5335594					
3--16	5.08	2.88	772.18713	39.5847241					
3--17	5.13	2.76	842.29272	44.6167429					
3--18	5.03	2.73	789.66803	43.1295758					
3--19	4.96	2.72	710.37085	39.4907894					
3--22	5.05	2.61	778.37286	44.2911608					
3--23	5.04	2.59	757.61908	43.5293183					
3--24	5.10	2.54	793.61694	45.9481786					
Sample #	Width	Thickness							
4--1	5.01	2.66	823.64111	46.3532208		Maximum	858.5603	4716.96914	46.60068
4--2	5.06	2.68	833.54395	46.1003748		Minimum	707.04675	418.13829	41.09521
4--3	5.07	2.70	802.36438	43.9603539		Mean	803.54178	3049.96552	44.035
4--6	5.09	2.76	845.85834	45.1577229		Standard Deviation	42.91444	1282.02723	1.80009
4--7	5.06	2.79	846.30811	44.9609052		Coefficient of Variation	5.34066	42.03415	4.08787
4--8	5.09	2.79	826.2337	43.6357236					
4--9	5.03	2.84	820.50134	43.0778712					
4--10	5.05	2.83	829.0719	43.5086537					
4--11	5.06	2.84	789.53888	41.206519					
4--14	5.03	2.83	858.5603	45.2353178					
4--15	4.96	2.80	838.67395	45.2912919					
4--16	5.02	2.79	798.39819	42.7536194					
4--17	5.04	2.69	823.0285	45.5295462					
4--18	5.01	2.67	761.63776	42.7032317					
4--19	5.00	2.65	726.01544	41.0952136					
4--22	5.04	2.55	707.04675	41.2608981					
4--23	5.00	2.53	755.09808	44.7686609					
4--24	5.01	2.50	778.23138	46.6006814					

LAMINATE:	F								
INJ Date	12/2/2014								
INJ PRESSURE	1.2	Bar							
							Maximum Flexure load (N)	Modulus (Automatic) (MPa)	Short Beam Strength
Sample #	Width	Thickness	Load	SBS					
5--1	4.92	2.57	817.37347	48.4823402		Maximum	853.1601	4296.39782	48.48234
5--2	5.06	2.58	834.71655	47.9545771		Minimum	710.59595	283.73776	41.20255
5--3	5.05	2.62	789.19849	44.735762		Mean	786.66967	2010.21902	44.20119
5--6	5.08	2.68	788.4126	43.4326485		Standard Deviation	43.1289	1515.25954	1.99822
5--7	5.07	2.68	801.50494	44.2409774		Coefficient of Variation	5.48247	75.37783	4.52075
5--8	5.08	2.69	750.72144	41.2025495					
5--9	5.06	2.72	778.90253	42.4448455					
5--10	5.04	2.73	792.56445	43.2018822					
5--11	5.11	2.73	843.30646	45.338082					
5--14	5.02	2.72	797.62695	43.8115342					
5--15	5.09	2.72	848.38281	45.9585626					
5--16	5.11	2.71	853.1601	46.2063442					
5--17	5.07	2.62	787.01654	44.4360935					
5--18	5.04	2.61	768.23083	43.8007908					
5--19	5.05	2.60	744.64099	42.53471					
5--22	4.93	2.55	735.38531	43.8721698					
5--23	5.03	2.53	710.59595	41.8789211					
5--24	5.12	2.50	718.31366	42.088691					
Sample #	Width	Thickness							
6--1	5.05	2.51	794.55591	47.013288		Maximum	896.33044	4611.37602	47.01329
6--2	5.14	2.53	774.22217	44.6522375		Minimum	702.8996	341.45923	35.9385
6--3	0	0	0			Mean	772.69622	2213.25211	42.20811
6--6	5.01	2.6	710.22223	40.8925743		Standard Deviation	47.6002	1584.90898	3.0235
6--7	5.05	2.61	736.85089	41.9284676		Coefficient of Variation	6.16027	71.60996	7.16331
6--8	5.15	2.62	803.93384	44.6861617					
6--9	5.13	2.66	770.237	42.3337401					
6--10	5.04	2.65	754.76868	42.383686					
6--11	4.94	2.65	776.35205	44.478194					
6--14	4.81	2.64	744.61902	43.9791048					
6--15	4.98	2.64	770.66248	43.9634949					
6--16	5	2.63	809.85193	46.1892736					
6--17	6.34	2.57	841.06586	38.714075					
6--18	5.73	2.56	702.8996	35.9385021					
6--19	5.84	2.53	741.33484	37.6307008					
6--22	5.78	2.49	770.96594	40.1762382					
6--23	5.65	2.45	736.96289	39.9293601					
6--24	6.46	2.44	896.33044	42.6488244					

B.2 ILSS Laminates G-H

Laminate:									max load kN	comments	avg b	sd b	avg w	sd w		IILSS
ACAB	Flow Rate		b1	b2	b3	w1	w2	w3	kN		mm	mm	mm	mm		tau (N/mm2
G	100cc/min	1-4	19.3	19.25	19.28	4.03	4.02	4.01	4.516		19.27667	0.025166	4.02	0.01		43.71
		1-5	18.99	18.86	18.73	4.03	4.03	4	4.067		18.86	0.13	4.02	0.017321		40.23
		1-6	19.05	19.02	19.04	3.98	3.97	4.03	4.112		19.03667	0.015275	3.993333	0.032146		40.57
		1-9	19.12	19.14	19.17	3.99	3.99	4.03	4.058		19.14333	0.025166	4.003333	0.023094		39.71
		1-10	19.26	19.28	19.28	3.98	3.99	4.01	4.229		19.27333	0.011547	3.993333	0.015275		41.21
		1-11	19.35	19.36	19.36	4.01	4.03	4.06	4.376		19.35667	0.005774	4.033333	0.025166		42.04
		2-4	19.85	19.86	19.89	3.98	3.99	4	4.09		19.86667	0.020817	3.99	0.01		38.70
		2-5	19.89	20.11	20.1	3.95	3.94	3.98	4.504	double	20.03333	0.124231	3.956667	0.020817		42.62
		2-6	20.04	20.06	20.12	3.9	3.93	3.95	4.389	double	20.07333	0.041633	3.926667	0.025166		41.76
		2-9	20.08	20.13	20.09	3.92	3.97	3.91	4.069		20.1	0.026458	3.933333	0.032146		38.60
		2-10	20.1	20.14	20.09	3.94	3.94	3.97	4.332		20.11	0.026458	3.95	0.017321		40.90
		2-11	20.03	20.04	20.03	4.03	4.02	3.98	4.224	double	20.03333	0.005774	4.01	0.026458		39.44
		3-4	20	20.01	20	4.03	4.02	4	3.77		20.00333	0.005774	4.016667	0.015275		35.19
		3-5	20	20.02	20.03	3.97	3.97	4.01	4.043		20.01667	0.015275	3.983333	0.023094		38.03
		3-6	20.02	20.03	20.04	3.94	3.95	3.94	4.051		20.03	0.01	3.943333	0.005774		38.47
		3-9	20	20.01	20.01	3.93	3.93	3.95	4.096		20.00667	0.005774	3.936667	0.011547		39.00
		3-10	20	19.99	20	3.95	3.95	3.97	4.026	double	19.99667	0.005774	3.956667	0.011547		38.16
		3-11	19.96	19.97	19.97	4	3.98	3.98	4.038	double	19.96667	0.005774	3.986667	0.011547		38.05
		4-4	19.88	19.83	19.72	4	4.01	4.01	3.723		19.81	0.081854	4.006667	0.005774		35.18
		4-5	20.03	20.02	19.99	4.01	4	3.97	3.974		20.01333	0.020817	3.993333	0.020817		37.29
		4-6	20.02	20.03	20.02	3.98	3.98	3.95	3.83		20.02333	0.005774	3.97	0.017321		36.14
		4-9	20.04	20.05	20.04	3.93	3.96	3.99	4.003		20.04333	0.005774	3.96	0.03		37.83
		4-10	20.01	20.03	20.03	3.97	3.97	3.96	3.914		20.02333	0.011547	3.966667	0.005774		36.96
		4-11	20	20.03	20.01	3.99	4.02	3.97	3.928	double	20.01333	0.015275	3.993333	0.025166		36.86
		5-4	19.98	19.96	19.84	4	4	4.02	3.558	double	19.92667	0.075719	4.006667	0.011547		33.42
		5-5	19.97	20.04	20.09	3.98	3.98	3.99	3.949		20.03333	0.060277	3.983333	0.005774		37.11
		5-6	20.01	20.04	20.02	3.96	3.95	3.97	3.977	double	20.02333	0.015275	3.96	0.01		37.62
		5-9	19.98	20	19.99	3.98	3.95	3.95	3.928	double	19.99	0.01	3.96	0.017321		37.22
		5-10	19.95	19.96	19.97	3.98	3.99	3.95	3.858		19.96	0.01	3.973333	0.020817		36.48
		5-11	19.94	19.95	19.94	3.98	3.98	4.01	4.058		19.94333	0.005774	3.99	0.017321		38.25
		6-4	20.06	20.04	20.07	4.04	4.04	4.06	3.776		20.05667	0.015275	4.046667	0.011547		34.89
		6-5	19.88	19.94	19.97	3.99	3.98	4.02	3.679		19.93	0.045826	3.996667	0.020817		34.64
		6-6	20	20	19.98	3.96	3.96	3.96	3.591	smooth	19.99333	0.011547	3.96	5.44E-16		34.02
		6-9	19.97	19.97	20	3.95	3.96	3.98	3.63	uble+smo	19.98	0.017321	3.963333	0.015275		34.38
		6-10	19.95	19.95	19.97	3.98	3.97	4	3.693	uble+smo	19.95667	0.011547	3.983333	0.015275		34.84
		6-11	19.96	20	19.96	4.01	4.03	4.01	3.58		19.97333	0.023094	4.016667	0.011547		33.47
		7-4														
		7-5														
		7-6														
		7-9	19.63	19.63	19.63	3.98	3.97	3.97	3.442	not saved	19.63	0	3.973333	0.005774		33.10
		7-10	19.68	19.69	19.69	3.97	3.99	4.02	3.666	double	19.68667	0.005774	3.993333	0.025166		34.97
		7-11	19.91	19.81	19.78	4.03	4.02	4	3.751	double	19.83333	0.068069	4.016667	0.015275		35.31

Laminate:									max load kN	comments	avg b	sd b	avg w	sd w	IILSS
ACAB	Flow Rate		b1	b2	b3	w1	w2	w3	kN		mm	mm	mm	mm	tau (N/mm2)
H	400cc/min	12	19.87	20.07	20	4.1	4.04	4.06	4.722		19.98	0.101489	4.066667	0.030551	43.59
		13	20.1	20.09	20.1	4.04	4.04	4.13	4.733		20.09667	0.005774	4.07	0.051962	43.40
		14	20.27	20.32	20.3	4.03	4.01	4.01	4.721		20.29667	0.025166	4.016667	0.011547	43.43
		16	20.53	20.49	20.5	4.01	4.02	4.02	4.648		20.50667	0.020817	4.016667	0.005774	42.32
		17	20.6	20.58	20.6	4.05	4.02	4.03	5	after this	20.59333	0.011547	4.033333	0.015275	45.15
		18	20.61	20.62	20.63	4.06	4.05	4.06	4.786		20.62	0.01	4.056667	0.005774	42.91
		22	19.82	19.84	19.81	3.99	3.99	3.99	4.726		19.82333	0.015275	3.99	0	44.81
		23	19.67	19.68	19.69	3.96	3.97	3.96	4.362	double	19.68	0.01	3.963333	0.005774	41.94
		24	19.63	19.61	19.63	3.93	3.94	3.93	4.562		19.62333	0.011547	3.933333	0.005774	44.33
		26	19.57	19.56	19.57	3.95	3.94	3.95	4.588		19.56667	0.005774	3.946667	0.005774	44.56
		27	19.5	19.49	19.45	3.97	3.97	3.97	4.521		19.48	0.026458	3.97	0	43.84
		28	19.13	19.15	19.19	4.04	3.98	4.01	4.571		19.15667	0.030551	4.01	0.03	44.63
		32	19.91	19.92	19.92	3.96	4.02	4.02	4.432		19.91667	0.005774	4	0.034641	41.72
		33	19.89	19.96	19.89	3.95	3.95	3.94	4.346		19.91333	0.040415	3.946667	0.005774	41.47
		34	19.84	19.86	19.85	3.91	3.95	3.94	4.632		19.85	0.01	3.933333	0.020817	44.49
		36	19.77	19.78	19.77	3.94	3.93	3.92	4.463		19.77333	0.005774	3.93	0.01	43.07
		37	19.78	19.79	19.79	3.94	3.95	3.97	4.412		19.78667	0.005774	3.953333	0.015275	42.30
		38	19.81	19.83	19.83	3.99	4.02	3.97	4.495		19.82333	0.011547	3.993333	0.025166	42.59
		42	19.93	19.94	19.94	3.96	3.96	3.99	4.392	double	19.93667	0.005774	3.97	0.017321	41.62
		43	19.87	19.89	19.88	3.94	3.94	3.97	4.486		19.88	0.01	3.95	0.017321	42.85
		44	19.83	19.82	19.82	3.92	3.93	3.93	4.136	double	19.82333	0.005774	3.926667	0.005774	39.85
		46	19.77	19.77	19.79	3.92	3.96	3.95	4.425		19.77667	0.011547	3.943333	0.020817	42.56
		47	19.78	19.78	19.79	3.94	3.95	3.95	4.386		19.78333	0.005774	3.946667	0.005774	42.13
		48	19.81	19.84	19.86	3.96	3.98	3.96	4.782		19.83667	0.025166	3.966667	0.011547	45.58
		52	19.88	19.89	19.89	3.98	4	3.96	4.667		19.88667	0.005774	3.98	0.02	44.22
		53	19.68	19.71	19.75	4	3.94	3.95	4.114		19.71333	0.035119	3.963333	0.032146	39.49
		54	19.5	19.5	19.5	3.92	3.92	3.96	3.968		19.5	0	3.933333	0.023094	38.80
		56	19.65	19.64	19.65	3.94	3.93	3.94	4.266		19.64667	0.005774	3.936667	0.005774	41.37
		57	19.67	19.68	19.68	3.98	3.96	3.95	4.411		19.67667	0.005774	3.963333	0.015275	42.42
		58	19.73	19.75	19.75	4.02	4.02	3.97	4.468		19.74333	0.011547	4.003333	0.028868	42.40
		62	19.96	19.95	19.96	4	4.05	3.97	4.175	smooth	19.95667	0.005774	4.006667	0.040415	39.16
		63	19.85	19.91	19.89	4.01	3.99	3.97	3.942		19.88333	0.030551	3.99	0.02	37.27
		64	19.81	19.8	19.81	3.96	3.98	3.94	4.008		19.80667	0.005774	3.96	0.02	38.33
		66	19.86	19.81	19.78	3.95	3.95	3.97	3.95		19.81667	0.040415	3.956667	0.011547	37.78
		67	19.75	19.74	19.8	3.96	3.96	4.01	4.082	smooth	19.76333	0.032146	3.976667	0.028868	38.95
		68	19.83	19.82	19.81	3.99	3.98	4.04	4.018	smooth	19.82	0.01	4.003333	0.032146	37.98
		72	19.89	19.9	19.91	4.02	4.03	4.05	3.993	smooth	19.9	0.01	4.033333	0.015275	37.31
		73	19.87	19.9	19.88	4	4.02	4.03	3.903		19.88333	0.015275	4.016667	0.015275	36.65
		74	19.8	19.78	19.82	3.98	3.98	3.99	3.99		19.8	0.02	3.983333	0.005774	37.94
		76	19.72	19.74	19.75	3.99	3.97	3.97	3.892		19.73667	0.015275	3.976667	0.011547	37.19
		77	19.69	19.69	19.67	4	4.01	4.01	3.807		19.68333	0.011547	4.006667	0.005774	36.20
		78	19.6	19.62	19.61	4.02	4.03	4.02	3.825	smooth	19.61	0.01	4.023333	0.005774	36.36

APPENDIX C. C-SCAN IMAGES

C.1 C-Scan Images Laminates C-F

Laminate C:

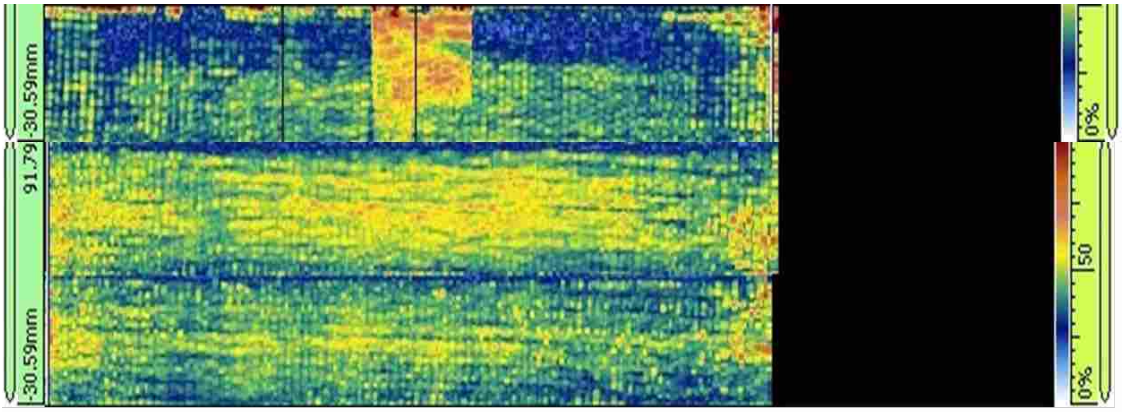

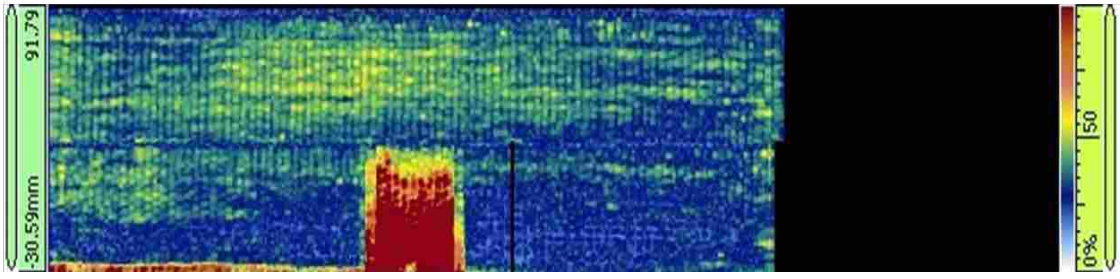

Laminate D:

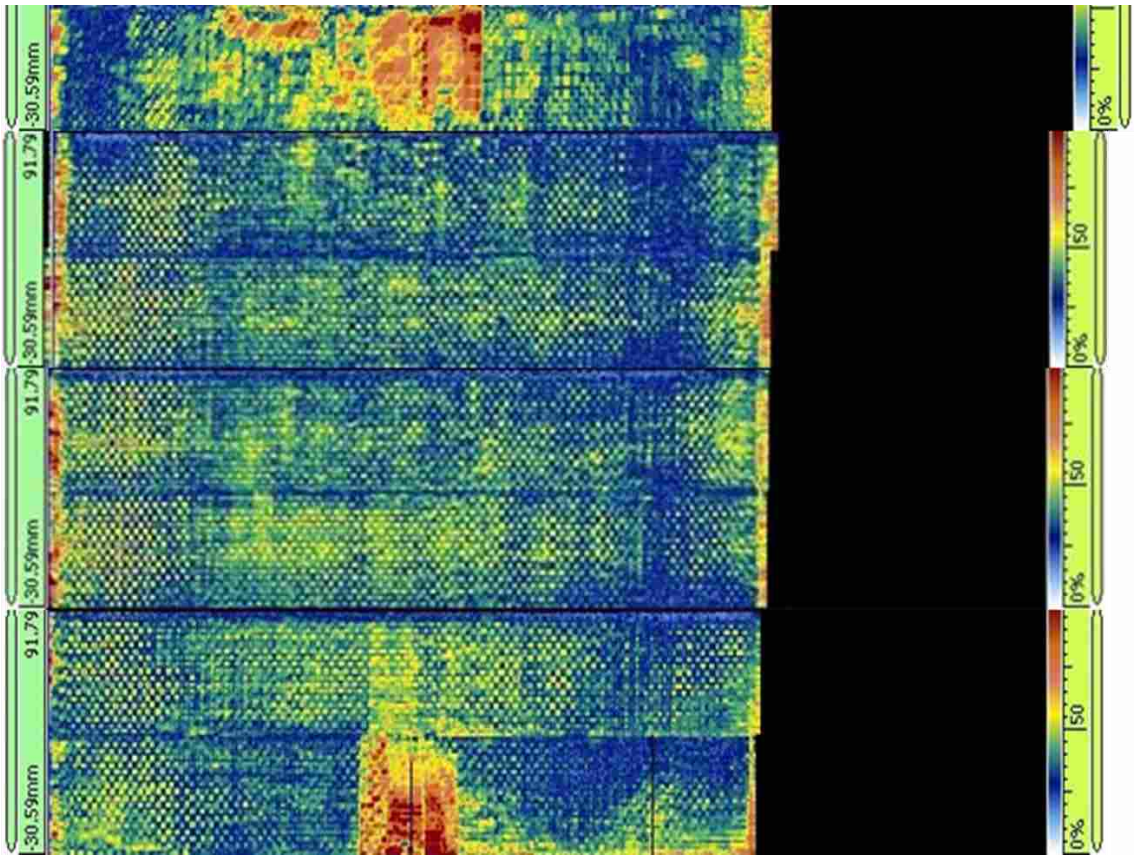

Laminate E:

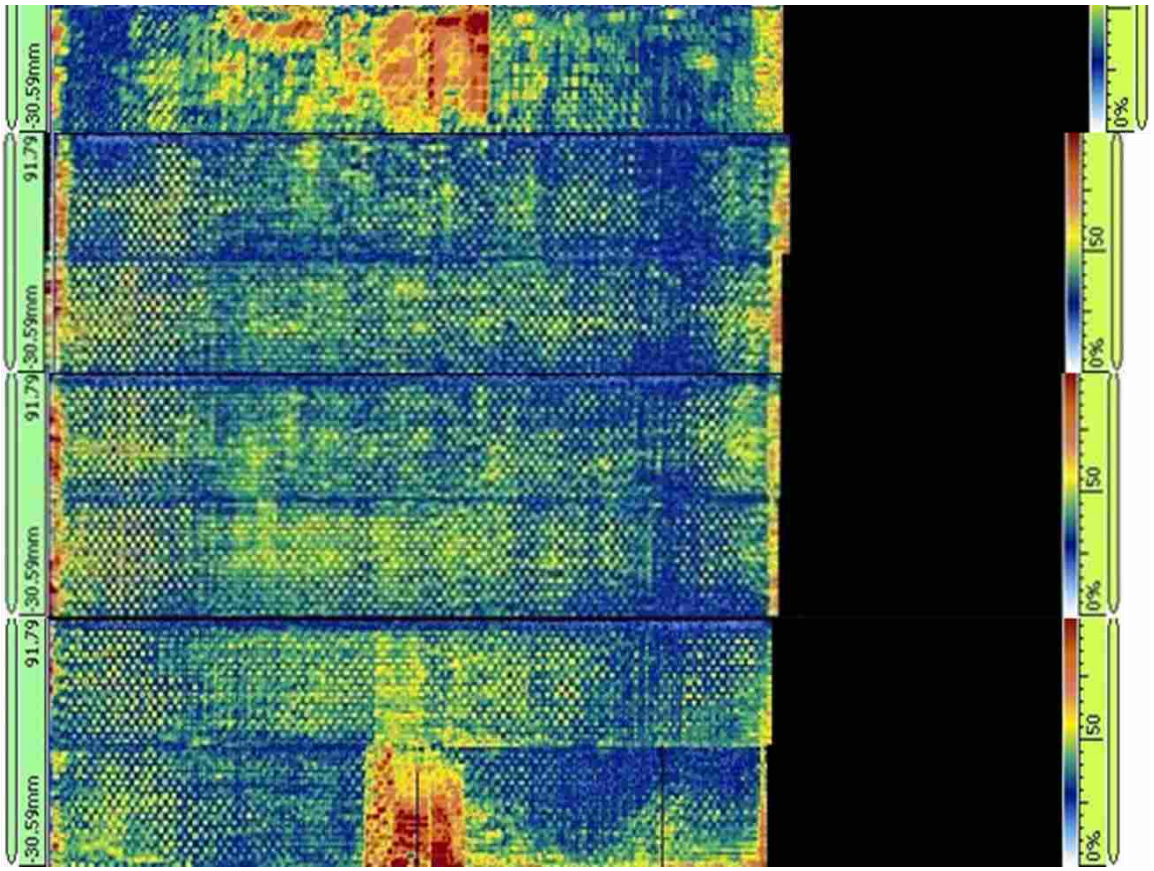

Laminate F: